NISTIR 6727

Use of Fluorescence to Measure the Lubricant Excess Surface Density During Pool Boiling

Mark A. Kedzierski

U. S. DEPARTMENT OF COMMERCE
Technology Administration
National Institute of Standards
and Technology
Building and Fire Research Laboratory
Gaithersburg, MD 20899-8230

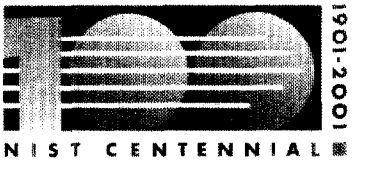

National Institute of Standards and Technology
Technology Administration
U.S. Department of Commerce

NISTIR 6727

Use of Fluorescence to Measure the Lubricant Excess Surface Density During Pool Boiling

Mark A. Kedzierski

U. S. DEPARTMENT OF COMMERCE
Technology Administration
National Institute of Standards
and Technology
Building and Fire Research Laboratory
Gaithersburg, MD 20899-8230

January 2001

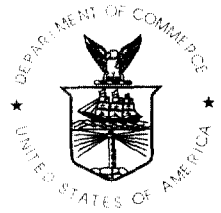

U.S. DEPARTMENT OF COMMERCE
Donald L. Evans, Secretary

NATIONAL INSTITUTE OF STANDARDS
AND TECHNOLOGY
Dr. Karen H. Brown, Acting Director

Use of Fluorescence to Measure the Lubricant Excess Surface Density During Pool Boiling

M. A. Kedzierski
National Institute of Standards and Technology
Bldg. 226, Rm B114
Gaithersburg, MD 20899
Phone: (301) 975-5282
Fax: (301) 975-8973

ABSTRACT

This paper presents what are believed to be the first measurements of the non-adiabatic lubricant excess surface density on a roughened, plain horizontal pool-boiling surface. Pool boiling heat transfer data is given for pure R123 and a R123/lubricant mixture. Lubricant excess surface density data is given for the boiling R123/lubricant mixture. A spectrofluorometer was used to measure the lubricant excess density that was established by the boiling of a R123/lubricant mixture on a test surface. The fluorescent measurement technique was used to confirm the existence of the lubricant excess layer during refrigerant/lubricant mixture boiling. The lubricant is preferentially drawn out of the bulk refrigerant/lubricant mixture by the boiling process and accumulates on the surface in excess of the bulk concentration. The excess lubricant resides in a very thin layer on the surface and influences the boiling performance. Accordingly, the ability to measure the lubricant excess density on the heat transfer surface would lead to a fundamental understanding of the mechanism by which lubricants can degrade or improve boiling performance. In support of this effort, heat transfer data are provided for both pure R123 and an R123/lubricant (1.8 % lubricant mass fraction) mixture at 277.6 K. The heat transfer data shows that the lubricant excess causes an average degradation of 12 % in the heat flux for a given superheat.

Keywords: adsorption, alternative refrigerants, boiling, enhanced heat transfer, fluorescence, non-adiabatic lubricant excess surface density, pool boiling, R123, reflected harmonic, refrigerant/lubricant mixtures, smooth surface, surfactant
[1]

[1] Certain trade names and company products are mentioned in the text or identified in an illustration in order to adequately specify the experimental procedure and equipment used. In no case does such an identification imply recommendation or endorsement by the National Institute of Standards and Technology, nor does it imply that the products are necessarily the best available for the purpose.

INTRODUCTION

It has been speculated that the pool boiling enhancement/degradation mechanism associated with the addition of a lubricant to refrigerant is due to an accumulation of lubricant at the boiling surface (Kedzierski 1993, Kedzierski and Kaul 1993, and Kedzierski 2001). Stephan (1963) was one of the first researchers to note that a lubricant-rich layer exists near the tube wall. The excess concentration (excess surface density) arises from the relatively low vapor pressure of the lubricant when compared to refrigerant. The lubricant can be locally drawn out of solution as a consequence of refrigerant evaporation at the heat transfer surface. The refrigerant/lubricant liquid mixture travels to the heated wall, and the refrigerant preferentially evaporates from the surface leaving behind a liquid phase enriched in lubricant. A balance between deposition and removal of the lubricant establishes some unknown thickness of the excess lubricant at the surface. It is hypothesized that the lubricant excess layer establishes the bubble size, the site density and, in turn, the magnitude of the heat transfer.

The enhancement mechanism of lubricants is analogous to the action of surfactants in that both enhancements arise from the creation of an excess layer. Kedzierski (1999) measured a significant enhancement of R123 pool boiling with the addition of 1 % and 2 % hexane mass fraction to R123. He used the Gibbs adsorption equation (Rosen, 1978) and the Young and Dupre equation (Adamson, 1967) to speculated that the boiling heat transfer enhancement of R123 by the addition of hexane was caused by an accumulation of hydrocarbon at the boiling surface. In essence, the greater concentration of hydrocarbon or "excess layer" at the heat transfer surface caused a reduction of the surface energy between the solid surface and the liquid. The existence of an excess layer at the liquid-solid interface is analogous to the existence of a surfactant induced excess layer at a liquid-vapor interface. Consequently, hydrocarbons and lubricants are not typical surfactants because they accumulate at the solid-liquid interface rather than at the liquid-vapor interface. However, the reduction in the liquid-solid surface energy results in a similar reduction in bubble departure diameter that occurs with a conventional surfactant. As a consequence of the bubble size reduction, the active site density increases. A heat transfer enhancement exists when a favorable balance between an increase in site density and a reduction in bubble size occurs.

Several measurement techniques exist to measure the bulk lubricant concentration in a refrigerant (Navarro de Andrade et al., 1999). These techniques rely on the measurement of various properties of the lubricant: density, light absorption, viscosity, and speed of sound. For example, Navarro de Andrade et al. (1999), Meyer and Saiz Jabardo (1994), and Baustian et al. (1988a) used temperature and speed of sound measurements of a liquid refrigerant/lubricant mixture to determine the bulk concentration of the mixture. Baustian et al. (1988b) used a bypass viscometer to correlate the mixture viscosity to the flowing lubricant concentration. Suzuki et al. (1993) used the light absorption properties of lubricant to quantify the fraction of lubricant in the refrigerant. Finally, Baustian et al. (1988c) and Bayani et al. (1995) demonstrated the use of a flowmeter densimeter to measure the concentration of lubricant in the liquid line of a refrigeration system. All of these methods are more suited for the measurement of the bulk lubricant concentration of

a non-boiling fluid rather than that of the localized lubricant excess layer, which cannot be measured with a global measurement technique.

With the purpose of confirming the existence of the lubricant excess layer on a boiling heat transfer surface, Kedzierski et al. (1998) proposed an in situ measurement technique that relied on the fluorescent properties of the lubricant. The proposed method relied on the relative fluorescent properties of the lubricant and the refrigerant. Ideally, the lubricant should strongly fluoresce while the refrigerant should not be fluorescent. In this way, the amount of lubricant in the mixture can be calculated from the intensity of the fluorescence emission. The Kedzierski et al. (1998) study demonstrated that the fluorescence intensity of a lubricant/methanol film on an adiabatic surface could be measured and that the intensity of the fluorescence increased with lubricant concentration. The study also proposed that the lubricant excess layer could be measured for a non-adiabatic boiling surface with a bifurcated optical bundle probe.

The present study describes the development of the fluorescence measurement technique for an actual pool-boiling surface. In the present study, pure R123 and a R123/lubricant mixture were tested in an effort to confirm the existence of the lubricant excess layer, and to investigate the influence of heat flux on the lubricant surface density. A naphthenic mineral oil (York-C™) was chosen for its somewhat favorable fluorescence characteristics and to demonstrate the new measurement technique with a commercial lubricant.

APPARATUS

Figure 1 shows a schematic of the apparatus that was used to measure the pool boiling data of this study. More specifically, the apparatus was used to measure the liquid saturation temperature (T_s), the average pool-boiling heat flux (q''), the wall temperature (T_w) of the test surface, and the fluorescence intensity from the boiling surface (F). The three principal components of the apparatus were test chamber, condenser, and purger. The internal dimensions of the test chamber were 25.4 mm × 257 mm × 1.54 m. The test chamber was charged with approximately 7 kg of R123 from the purger, giving a liquid height of approximately 80 mm above the test surface. As shown in Fig. 1, the test section was visible through two opposing, flat 150 mm × 200 mm quartz windows. The bottom of the test surface was heated with high velocity (2.5 m/s) water flow. The vapor produced by liquid boiling on the test surface was condensed by the brine-cooled, shell-and-tube condenser and returned by gravity to the liquid pool.

Figure 2 shows a view of the spectrofluorometer that was used to make the fluorescence measurements and the test chamber with the fluorescence probe perpendicular to the heat transfer surface. Figure 3 shows a simplified schematic of the right angle spectrofluorometer consisting of a xenon light source, an excitation and an emission monochromator, and an emission photomultiplier tube (detector). The light source was focused into the excitation monochromator by a collimating lens. The monochromator was set to emit light at a wavelength of 380 nm. Because the intensity of the xenon lamp varies with wavelength, a corrected excitation module was used to compensate for the variation. The light from the excitation monochromator passed through a 2.5 nm slit

before it entered the sample chamber. All of the slit widths were 2.5 nm to limit the bandwidth of the wavelength. The spectrofluorometer was designed to accept 45 mm × 10 mm × 10 mm fluorescent samples or cuvettes filled with fluorescent material. A special adapter with lenses and mirrors, which replaced the cuvette holder, was fabricated to allow the optical bundles to communicate with the standard sample chamber of the spectrofluorometer. The adapter was configured to direct excitation light to the test surface and the emission light from the test surface to the detector. A glass filter was placed before the emission monochromator to keep light with wavelengths less than 420 nm from entering it. The emission monochromator was used to select the optimum wavelength to measure the fluorescent intensity. The intensity of the emission was measured with a photomultiplier tube and accompanying electronics. This light was then directed to the detector that produces a voltage signal proportional to the intensity of the fluorescence.

The fluorescence probe shown in Fig. 2 was a bifurcated optical bundle with 168 fibers spanning from the spectrofluorometer to the test surface. Two optical bundles consisting of 84 fibers each originated from the spectrofluorometer. One of the bundles transmitted the excitation light to the test surface. The other bundle carried the emission from the test surface to the spectrofluorometer. The optical bundles originating from the spectrofluorometer merged into a single probe before entering the test section chamber. The sensor end of the fluorescence probe was sheathed with a quartz tube to protect it from reacting with the R123 test fluid. The 168 fibers of the probe were split evenly between the fibers to transmit the incident intensity (I_o) to the test surface and those to receive the fluorescence intensity (F) from the lubricant on the test surface. The transmitting and sending fibers were arranged randomly with respect to one another.

To reduce the errors associated with the liquid saturation temperature measurement, the saturation temperature of the liquid was measured with two 450 mm long, 1.6 mm diameter stainless steel sheathed thermocouples. The small diameter provided for a relatively rapid response time. Nearly the entire length of the thermocouple was in contact with either the test refrigerant vapor or liquid to minimize conduction errors. The tip of the two thermocouples were placed approximately 2 mm above and 150 mm (and 300 mm) to one side of the top of the test surface. This placement ensured that approximately 80 mm of the probe length was in relatively well-mixed liquid near the two-phase fluid above the test surface. To provide for a saturated liquid pool state, the mass of liquid in the pool was large compared to mass of liquid condensed. At the highest heat flux, it would require nearly one hour to evaporate and condense the entire test chamber charge. The lack of a temperature difference between the probe and the well-insulated, low emissivity, 38 mm aluminum test chamber walls essentially eliminated temperature errors due to radiation to the probe.

TEST SURFACE

Figure 4 shows the oxygen-free high-conductivity (OFHC) copper flat test plate used in this study. The test plate was machined out of a single piece of OFHC copper by electric discharge machining (EDM). A tub grinder was used to finish the heat transfer surface of the test plate with a crosshatch pattern. Figure 5 shows a photograph of the crosshatch

surface with sample roughness traces for the longitudinal and the diagonal directions. The longitudinal trace depicts the gross overall roughness of the surface from groove to groove. The diagonal trace characterizes the local roughness within a particular groove. Both traces were measured with a stylus having a 0.8 μm tip radius and 100 mgf of applied force. This gave a roughness resolution of approximately 10 nm. A 2.5 mm filter cut off length and a 12.5 mm traversing length was used for the longitudinal traces in the y-direction. A smaller traversing length (0.4 mm) and cut off length (0.08 mm) were used for the diagonal traces. The average R_a roughness[2] and the mean peak spacing parameter (S_m) of three longitudinal traces were 3.39 μm and 139 μm, respectively. The average R_a roughness and the S_m of five diagonal traces were 0.96 μm and 50.4 μm, respectively. The S_m is approximately twice the average cavity diameter for bubble nucleation. Consequently, an estimate of the approximate range of average cavity radii for the surface is 12 μm to 35 μm. The gross roughness of the surface measured by the longitudinal trace was much more uniform than that of the roughness within the grooves. The relative standard uncertainty of the R_a and S_m measurements for the longitudinal trace was 1.2 % and 9 %, respectively, compared to 52 % and 15 %, respectively, for the diagonal measurement.

MEASUREMENTS AND UNCERTAINTIES

The standard uncertainty (u_i) is the positive square root of the estimated variance u_i^2. The individual standard uncertainties are combined to obtain the expanded uncertainty (U). The expanded uncertainty is calculated from the law of propagation of uncertainty with a coverage factor. All measurement uncertainties are reported for a 95 % confidence interval except where specified otherwise.

Heat Transfer

The copper-constantan thermocouples and the data acquisition system were calibrated against a glass-rod standard platinum resistance thermometer (SPRT) and a reference voltage to a residual standard deviation of 0.005 K. The NIST Thermometry Group calibrated the fixed SPRT to two fixed points having expanded uncertainties of 0.06 mK and 0.38 mK. A quartz thermometer, which was calibrated with a distilled ice bath, agreed with the SPRT temperature to within approximately 0.003 K. Both the measured thermocouple electromotive force (EMF) and the measured 1 mV reference were regressed to the SPRT temperature. During a pool-boiling test, the 1 mV reference was measured prior to measuring each thermocouple EMF. The reference voltage was used to account for the drift in the acquisition measurement capabilities over time. Before each test run, the measurements of a thermocouple in the bath with the SPRT were compared. The thermocouple calibration was then adjusted so that bath thermocouple and the SPRT agreed. The mean absolute difference between the thermocouple and the SPRT before correcting for the drift was consistently around 0.07 K over a year of testing. Considering the fluctuations in the saturation temperature during the test and the standard uncertainties in the calibration, the expanded uncertainty of the average saturation temperature was no greater than 0.04 K. Consequently, it is believed that the expanded uncertainty of the temperature measurements was less than 0.1 K. The saturation

[2] Vorburger and Raja (1990) provide clear definitions of roughness parameters.

temperature was also obtained from a pressure transducer measurement with an expanded uncertainty of less than 0.03 kPa. The uncertainty of the saturation temperature from a regression (with a residual standard deviation of 0.6 mK) of equilibrium data (Morrison and Ward, 1991) for R123 was 0.17 K. The saturation temperature obtained from the thermocouple and the pressure measurement nearly always agreed within ± 0.17 K for the pure R123 data.

Figure 4 shows the coordinate system for the 20 wells where individual thermocouples were force fitted into the side of the test plate. The wells were 16 mm deep to reduce conduction errors. Using a method given by Eckert and Goldstein (1976), errors due to heat conduction along the thermocouple leads were estimated to be well below 0.01 mK. The origin of the coordinate system was centered on the heat transfer surface with respect to the y-direction. Centering the origin in the y-direction improved the accuracy of the wall heat flux and temperature calculations by reducing the number of fitted constants involved in these calculations. The x-coordinate measures the distance normal to the heat transfer surface. The y-coordinate measures the distance perpendicular to the x-coordinate. The thermocouples were arranged in four sets of five aligned in the x-direction. Following a procedure given by Kedzierski and Worthington (1993), the size and arrangement of the thermocouple wells were designed to minimize the errors in the wall temperature and temperature gradient measurement.

The heat flux and the wall temperature were obtained by regressing the measured temperature distribution of the block to the governing two-dimensional conduction equation (Laplace equation). In other words, rather than using the boundary conditions to solve for the interior temperatures, the interior temperatures were used to solve for the boundary conditions following a backward stepwise procedure given in Kedzierski (1995).

A backward stepwise regression was used to determine the best model or the significant terms of the solution to the Laplace equation in rectangular coordinates for each data point. Most infinite series solutions should converge within nine terms. The backward stepwise method began by regressing the first nine terms of the Laplace infinite series solution to the twenty measured plate temperatures:

$$T = C_0 + C_1 x + C_2 y + C_3(x^2 - y^2) + 2C_4 xy + C_5 x(x^2 - 3y^2) + C_6 y(3x^2 - y^2) + C_7(x^4 - 6x^2 y^2 + y^4) + 4C_8(x^3 y - xy^3) \quad (1)$$

The above "full" model was reduced to its significant terms by removing terms with t-values less than two while maintaining the original residual standard deviation of the full model. Terms were removed one at a time. Regression of the 20 temperatures was done after each term with the smallest t-values was removed. Table 1 provides an overview of the various two-dimensional conduction models that were used to reduce the measured temperatures to heat fluxes and wall temperatures. The top three most frequently occurring models are given with the corresponding percentage of appearance.

Fourier's law and the fitted constants (C_0, C_1, ... C_n) were used to calculate the average

heat flux (q'') normal to and evaluated at the heat transfer surface as:

$$q'' = \left(\frac{1}{L_y} \int_{\frac{-L_y}{2}}^{\frac{L_y}{2}} k \frac{\partial T}{\partial x} dy \right)_{x=0} = \bar{k} C_1 \qquad 2$$

where $\bar{k}$ is the average thermal conductivity along the surface of the plate, and L_y is the length of the heat transfer surface as shown in Fig. 4.

The average wall temperature (T_w) was calculated by integrating the local wall temperature:

$$T_w = \left(\frac{1}{L_y} \int_{\frac{-L_y}{2}}^{\frac{L_y}{2}} T dy \right)_{x=0} = C_0 \qquad 3$$

Siu et al. (1976) estimated the uncertainty in the thermal conductivity of OFHC copper to be about 2 % to 3 % by comparing round-robin experiments. Considering this, the relative expanded uncertainty in the heat flux ($U_{q''}$) was greatest at the lowest heat fluxes, approaching 8 % of the measurement at 10 kW/m^2. In general, the $U_{q''}$ was relatively constant between 4 % and 5 % for heat fluxes above 25 kW/m^2. The average random error in the wall superheat (U_{Tw}) was between 0.02 K and 0.08 K. Plots of $U_{q''}$ and U_{Tw} versus heat flux can be found in Appendix A.

Fluorescence

Appendix B gives the details for transferring the analog wavelength and intensity measurements from the spectrofluorometer to the computer. Appendix C discusses how the emission and excitation wavelength measurements were verified with a mercury standard and a "crossover peak" from the excitation. The text that follows describes how the emission intensity measured with the spectrofluorometer was calibrated against the bulk lubricant mass fraction. This section also describes how the effect of the reflected excitation on the measured fluorescence emission signal was made inconsequential.

Figure 6 shows the vessel that was used to calibrate the fluorescence intensity received from the bifurcated optical bundle against lubricant mass fraction. The metal lid of the 150 mL glass jar had a port for evacuation and filling of the test sample and a fitting to seal around the glass tube that pierced the lid. The glass tube was the same type that was used in the test chamber of Fig. 2. A copper disk with the same roughness as the heat transfer test surface was placed on the bottom of the jar. By using the same material and surface roughness, the disk and the test plate had the same reflective properties. The distance between the top of the copper disk and the bottom of the glass tube was set with the aid of a 1.6 mm Teflon gauge disk. This fixed the mass of liquid below the probe so that the same amount of potentially fluorescent material was under the probe during the calibration as was during the actual heat transfer tests. The jar and the portion of the

glass rod above the lid were covered with black insulation to prevent the optical probe from receiving ambient light. The probe was focused to the maximum intensity for a given measurement so that most of the light was concentrated below the probe. The focused beam was achieved by manually sliding the optical probe in the glass tube.

Figure 7 shows the analysis of the emission and excitation spectra of pure York-C™ in a cuvette. The test sample was placed directly in the sample chamber of the right angle spectrofluorometer. The excitation wavelength that produced the maximum fluorescence emission was iteratively found by scanning through both excitation and emission wavelengths. The excitation and emission wavelengths for York-C™ that produced the largest intensities were located at 405 nm and 435 nm, respectively.

As the name suggests, right angle spectrometry was designed to limit the interference of the excitation signal on the emission signal by orientating the detector perpendicular to the beam of the emission monochromator. Considering this, the parallel configuration of the excitation and emission at the measuring end of the bifurcated optical bundle as shown in Figs. 2 and 6 is not ideal. The parallel configuration encourages the reflection of the excitation from the copper surface to be transmitted through the emission fiber optics and to the detector. This can be a serious limitation given that the reflected excitation can overwhelm the emission signal even if the emission wavelength (λ_m) and the excitation wavelength (λ_x) differ because: (1) the excitation intensity can be several orders of magnitude greater than that of the fluorescence emission, and (2) the filtering process of the emission monochromator is not complete enough to remove the entire reflected wave. The incomplete filtering process of the monochromator supplies the detector with an intensity that is distributed about the wavelength with comparatively negligible intensities except near the desired wavelength. Consequently, if the excitation intensity is very large, the tails of the excitation distribution can be greater than the peak emission intensity. This occurred with the bifurcated optical probe for the optimum wavelengths as dictated by the cuvette measurements, i.e., where the fluorescence was examined at 435 nm for an excitation wavelength of 405 nm.

A successful remedy for reducing the interference of the excitation signal was to place a 420 nm glass filter in front of the detector as shown in Fig. 3 and to put a greater separation between the excitation and the emission wavelengths. The glass filter reduced the intensity of the reflected excitation light that entered the emission monochromator. Further reduction in the reflection without much loss in emission intensity was accomplished by increasing the emission wavelength to 455 nm. Trials with the calibration vessel and the probe revealed that a 380 nm excitation produced a significantly large fluorescence intensity and an acceptably small reflection of the excitation. Consequently, all tests with the probe were excited at 380 nm while the emission was observed at 455 nm. The reflection that remained at these wavelengths was accounted for in the calibration of the spectrofluorometer, as outlined below, by setting the emission intensity for the pure R123 calibration jar to zero.

Three jars were used in the calibration of the bulk lubricant mass fraction to the fluorescent intensity. Two jars were used to set the lower (0) and upper (100) limits of

the intensity signal on the spectrofluorometer. A jar that contained only pure R123 was used to zero the intensity. Because light intensities are additive, the zeroing ensured that the reflected excitation wave and other effects were not attributed to fluorescence. A second jar that contained a 0.5 mass fraction[3] liquid mixture of R123 and York-C™ was used to set the intensity on the spectrofluorometer to 100. The 50/50 composition was arbitrarily chosen to ensure enough range in the bulk composition for a statistically adequate calibration. The third jar was used to measure and record the intensity of prepared refrigerant/lubricant mixtures of various concentrations. The third jar was initially charged with approximately 20 g of lubricant and then evacuated for approximately 10 s. Evacuation of the jar and the sample prevented fluorescence quenching by oxygen (Guilbault, 1967). The jar was then charged with approximately 20 g of pure R123 to give approximately a 0.5 mass fraction. Calibration measurements proceeded by successively diluting the mixture with approximately 2 g increments of pure R123.

A single calibration run consisted of measurements for concentrations beginning with a 0.5 mass fraction and diluting to a lubricant mass fraction of 0.05 or less. Prior to each emission intensity measurement for the variable jar, the zero and 100 limits for the emission intensity of the spectrofluorometer were set with the pure R123 jar and the 50/50 jar, respectively. All emission measurements were made at a wavelength of 455 nm with an excitation wavelength of 380 nm. Although, the calibration data was taken at room temperature, both the pure refrigerant jar and the 50/50 jar were maintained within approximately 1 K of the temperature of the saturated refrigerant in the boiling rig during heat transfer/fluorescence measurements to account for the temperature affect on fluorescence (Miller, 1981).

Figure 8 shows eight different calibration runs using the calibration procedure described above. The solid line depicts the regression of the intensity of the fluorescence emission (F) to the Beer-Lambert-Bougher law (Amadeo et al., 1971):

$$F = I_o(\lambda)\left[1-10^{-\varepsilon_\lambda cl}\right]\Phi \qquad 5$$

Here c is the concentration of the fluorescent substance, which can be rewritten as a product of the bulk lubricant mass fraction (x_m) and the bulk liquid mixture density (ρ_m) divided by the molar mass of the lubricant (M_L). The neat lubricant liquid density was measured in a pycnometer and is given in Appendix D. The mixture densities were calculated on a linear mass weighted basis. The quantum efficiency of the fluorescence (Φ), the extinction coefficient (ε), the path length (l), the intensity of the incident radiation (I_o), and the M_L are all unknowns that are lumped into two regression constants to give the regressed calibration of F_c against x_m:

$$F_c = 116\left[1-10^{-0.00159 x_m \rho_m}\right] \qquad 6$$

[3] Liquid composition assuming that some refrigerant but no lubricant is in the vapor phase.

The average 95% confidence interval for the lubricant mass fraction is approximately ± 0.01. The width of the confidence interval is a function of the lubricant fluorescence. A greater absolute fluorescence intensity would reduce the scatter in the data.

Because the molar mass of the lubricant is unknown, the surface excess density (Γ) is defined in this work on a mass basis as:

$$\Gamma = \rho_e x_e l_e - \rho_b x_b l_e \qquad 7$$

Precedence for reporting the surface excess density in mass units is given by citing the work of McBain and Humphreys (1932) in which they experimentally verified the Gibbs adsorption equation. A non-zero value of Γ implies that an excess layer exists on the surface.

The measured fluorescence emission intensity (F_m) is a sum of the intensity due to the lubricant in the bulk fluid below the probe (F_b) and the fluorescence intensity from the lubricant in the excess layer at the wall (F_e). A simplified form of the Beer-Lambert-Bougher law, valid more so for dilute solutions (Amadeo et al., 1971), was used to separate the fluorescence intensity of excess layer from the total intensity:

$$F = 2.3 I_o \varepsilon c l \Phi \rightarrow [\varepsilon c l \leq 0.05] \qquad 8$$

Equation 8 was written for the excess layer and normalized by eq 8 for the bulk fluid. The common constants canceled, and the normalized eq 8 was combined with $F_m = F_b + F_e$ and solved for the excess surface density (Γ):

$$\Gamma = \rho_e x_e l_e - \rho_b x_b l_e = \rho_b x_b \left\{ \frac{\frac{F_m}{F_c} - 1}{\frac{I_{oe}}{I_{ob}} \left(1 + 1.165 \frac{\varepsilon}{M_L} x_b \rho_b l_b \right) \frac{1}{l_b} - 1.165 \frac{\varepsilon}{M_L} x_b \rho_b \left(\frac{F_m}{F_c} - 1 \right)} - l_e \right\} \qquad 9$$

where the l_e is the thickness of the lubricant excess layer. The l_b is the distance between the probe and the wall and is taken as the thickness of the gauge disk because $l_b >> l_e$. The fluorescent intensity from the calibration (F_c) is obtained from eq 6 evaluated at the charged bulk lubricant concentration of test fluid in the boiling apparatus. The ratio of the absorption of the incident excitation in the bulk to that in the excess layer (I_{oe}/I_{ob}) was obtained from the measured absorption spectrum of a 95/5 mass fraction mixture of R123 and York-C™ shown in Fig. 9. A sample calculation of the absorption ratio for the 0.018 lubricant mass fraction mixture is given in Appendix E.

The two terms multiplied by 1.165 generalize the expression for the excess surface density so that it is valid for non-dilute solutions. The value of 1.165 was obtained from

a regression of the ratio of eq 5 to eq 8 against $\frac{\varepsilon}{M_L} x\rho l$. The value of $\frac{\varepsilon}{M_L}$ was obtained from the fluorescence calibration as 1.089 m^2/kg. The extinction coefficient was obtained from the absorption measurements as 0.23 m^2/mol at 455 nm. The molar mass of the lubricant was calculated from $\frac{\varepsilon}{M_L}$ and ε to be 211 g/mol, which is consistent with the molar mass of lower viscosity lubricants.

EXPERIMENTAL RESULTS

Heat Transfer

The heat flux was varied from approximately 80 kW/m^2 to 10 kW/m^2 to simulate typical operating conditions of R123 chillers. All pool-boiling tests were taken at 277.6 K saturated conditions. The data were recorded consecutively starting at high heat flux and descending in intervals of approximately 4 kW/m2. The descending heat flux procedure minimized the possibility of any hysteresis effects on the data, which would have made the data sensitive to the initial operating conditions. Table 2 presents the measured heat flux and wall superheat for all of the data of this study. Table 3 gives the number of test days and data points for each fluid.

The R123/mixture was prepared by charging the purger (see Fig. 1) with pure R123 to a known mass. Next, a measured weight of York-C™ was injected with a syringe through a port in the test chamber. The lubricant was mixed with R123 by flushing pure R123 through the same port where the lubricant was injected and releasing the R123 from the purger. All compositions were determined from the masses of the charged components and are given on a mass percent basis. The maximum uncertainty of the composition measurement is approximately 0.02 %, e.g. the range of a 1.8 % composition is between 1.78 % and 1.82 %.

Figure 10 is a plot of the measured heat flux (q") versus the measured wall superheat (T_w - T_s) for pure R123 at a saturation temperature of 277.6 K. The closed circles represent the present R123 "break-in" boiling data while the closed squares represent the present R123 "surface aged" boiling data. Measurements for each data set were made over a period of approximately one month in the same apparatus and for the same surface. The "surface-aged" boiling data was taken after a month hiatus in R123 "break-in" testing. The data differ substantially in the vigorous boiling region (5K superheat offset), but agree closely in the natural convection/boiling region. Apparently, the surface condition has changed such that many nucleation sites have been eliminated for the aged surface. Marto and Lepere (1982) have also observed a surface aging effect on pool boiling data that was sensitive to initial surface conditioning and fluid properties. The present surface was cleaned prior to installation in the test apparatus with acetone, Tarnex™, hot tap water, and acetone. Following the cleaning process, the surface was exposed to a heat lamp for several hours. It is believed that the superheat offset is not caused by a malfunctioning of the test equipment because no equivalent offset between the measured saturation temperature and the saturation temperature obtained from the measured

pressure was observed. Also, the agreement of low heat flux data for the two periods shows that the measurements are consistent.

The solid lines shown in Fig. 10 are cubic best-fit regressions or estimated means of the data. Two cubic fits were required to cover the low and the high heat flux data. Table 4 gives the constants for the cubic regression of the superheat versus the heat flux for each data set. The residual standard deviation of the regressions - representing the proximity of the data to the mean - are given in Table 5. Note that the residual standard deviation of the high heat flux data differs between the pure R123 and the R123 "break-in" data by about 50 %, i.e., 0.31 K and 0.20 K, respectively. The greater repeatability of the final set of pure R123 data suggests that the surface is operating in the "broken-in" condition. The dashed lines to either side of the mean represent the lower and upper 95 % simultaneous (multiple-use) confidence intervals for the mean. From the confidence intervals, the expanded uncertainty of the estimated mean wall superheat in the low heat flux region and the high heat flux region ranged between 0.17 K and 0.67 K with the mean of the data having a value of 0.24 K. Table 6 provides the average mean wall uncertainty for all of the test data.

Figure 10 shows that the boiling curve for pure R123 at 277.6 K on the plain surface exhibits two characteristic regimes: a natural convection/boiling regime and a vigorous nucleate boiling regime. The regimes are separated by the cessation of vigorous nucleate boiling (CVNB). The CVNB occurs for the pure R123 data at a superheat of approximately 14 K and 20 K for the "break-in" and surface aged data, respectively. The vigorous nucleate boiling regime exists for superheats that are greater than the CVNB condition. Here, the heat transfer is governed primarily by the formation of isolated bubbles within the cavities of the surface. The superheats below the CVNB are insufficient to support vigorous bubble generation. Consequently, natural convection becomes a prevalent mode of heat transfer for superheats below CVNB (low-active-site-density region). In this region, limited bubble activity exists.

Figure 10 also gives the smooth tube boiling curve measured by Webb and Pais (1992) at the same saturation temperature as the present tests. The Webb and Pais (1992) smooth tube superheat and the "surface aged" superheat agree within 3 K for the vigorous-boiling region. The Webb and Pais (1992) smooth tube heat flux data in the natural convection influenced region is approximately 40 % less than the heat flux for the "surface aged" data. Figure 10 also shows the predictions from a free convection correlation for a horizontal plate with the heated surface facing upward which was recommended by Incropera and Dewitt (1985). The predictions are substantially lower than the present measurements and the Webb and Pais (1992) data. This is consistent with the enhancement of the free convection by some nucleate boiling and the upward motion of bubbles.

Figure 11 plots the measured heat flux (q'') versus the measured wall superheat ($T_w - T_s$) for the R123/ York-C^{TM} (98.2/1.8) mixture at a saturation temperature of 277.6 K. The mean of the pure R123 "aged data" is plotted as a dashed line. The mean heat transfer performance of the refrigerant/lubricant mixture is less than that of the pure refrigerant

for all superheats. A more detailed comparison of the mixture and the pure fluid heat transfer performance is given in Fig. 12.

Figures 12 plots the ratio of the mixture to the pure R123 heat flux (q''_m/q''_p) versus the pure R123 heat flux (q''_p) at the same wall superheat. A heat transfer enhancement would exist if the heat flux ratio was greater than one and the 95 % simultaneous confidence intervals (depicted by shaded region) did not include the value one. Considering this, Fig. 12 shows that the R123/York-C™ (98.2/1.8) mixture exhibits a degradation for all the heat fluxes that were tested with the exception of heat fluxes between 28 kW/m^2 and 35 kW/m^2 where the heat transfer may not differ from the pure refrigerant. The CVNB for the mixture was visually observed to be located near 26 kW/m^2. Recall that the CVNB for pure R123 occurred at approximately 35 kW/m^2. Consequently, the addition of York-C™ to R123 enhances the boiling site density but this is not sufficient to cause an overall enhancement of the boiling performance due to the loss in bubble size with lubricant addition. The maximum heat flux ratio for the 98.2/1.8 mixture was 0.98 at 33 kW/m^2. The average heat flux ratio for the R123/York-C™ (98.2/1.8) mixture from 20 kW/m^2 to 54 kW/m^2 was 0.88.

Fluorescence

Although the heat flux was varied from approximately 80 kW/m^2 to 10 kW/m^2, fluorescence measurements were limited between 40 kW/m^2 and 10 kW/m^2 to ensure that boiling did not occur below the fluorescence probe. It was believed that bubbles could have misdirected the excitation and the emission lights. Boiling occurred in patches on the surface for the lower heat fluxes. Accordingly, the surface under the fluorescence probe was observed before fluorescence measurements were made to ensure that no boiling occurred under the probe.

The excess surface density was obtained from eq 9. Key inputs for eq 9 were the fluorescence intensity measurements (F_m) and the following expression for the excess layer thickness (l_e):

$$l_{e,min} = \frac{\frac{\rho_b x_b}{\rho_L}\left(\frac{F_m}{F_c}-1\right)}{\frac{I_{oe}}{I_{ob}}\left(1+1.165\frac{\varepsilon}{M_L}x_b\rho_b l_b\right)\frac{1}{l_b}-1.165\frac{\varepsilon}{M_L}x_b\rho_b\left(\frac{F_m}{F_c}-1\right)} \qquad \textbf{10}$$

Equation 10 represents the minimum thickness of the lubricant excess layer. A minimum thickness occurs for an excess layer composed of entirely lubricant. Small excess layer mass fractions give excess layers that are unrealistically too thick. For example, the excess layer thickness ranges from 0.7 mm to 1.3 mm for an assumed excess layer mass fraction of 0.03. Two physical mechanisms support a thin, neat lubricant layer: (1) the preferential evaporation of the refrigerant tends to enrich the excess layer in the lubricant phase; while (2) the bubble pumping action of lubricant from the surface tends to minimize the thickness of the lubricant excess layer. Consequently, it was assumed that the excess layer consisted of entirely lubricant, i.e., $x_e = 1$. As shown in Fig. 13, the resulting thickness of the non-adiabatic excess layer for $x_e = 1$ ranges from 0.04 mm to

0.06 mm depending on the heat flux. This gives an excess layer thickness that is approximately 100 times larger than one of the largest adiabatic film thickness (Kayser, et al. 1986). Apparently, preferential evaporation of refrigerant sustains lubricant excess layer thickness that are much thicker than that which would be possible by long-range van der Waals forces alone.

Figure 14 is a plot of the measured lubricant excess density versus the heat flux. The lubricant excess density is roughly the mass of lubricant in the excess layer per surface area in excess of the lubricant contribution from the bulk. Consequently, $\Gamma=0$ implies that no excess layer exists on the surface. Considering this, Fig. 14 substantiates the existence of the lubricant excess layer because the data, it's mean, and the confidence intervals for the mean are all greater than zero. The data also suggest that lubricant removal from the excess layer increases with heat flux by a greater rate than does lubricant deposition. As a result of increased lubricant removal, the thickness of the excess layer is shown in Fig. 13 to decreases with heat flux. Possibly the exponential increase in site density with respect to heat flux is responsible for this phenomenon assuming that the excess layer is removed from the surface as lubricant caps on bubbles. That is to say, lubricant removal is proportional to the site density, while the lubricant deposition is proportional to volume of vapor generated. Consequently, if the site density increases at a greater rate with increasing heat flux than does the vapor volume, then the lubricant removal will also increase at a greater rate with heat flux than does the lubricant deposition.

CONCLUSIONS

A fluorescent measurement technique was developed and has confirmed the existence of the lubricant excess layer during boiling of R123 and a commercial lubricant (York-C™). A spectrofluorometer was specially adapted for use with a bifurcated optical bundle so that fluorescence measurements could be made perpendicular to the heat transfer surface. The heat transfer surface was a horizontal, roughened, copper flat plate. The fluorescence emission intensity was calibrated against the bulk lubricant mass fraction using specially designed calibration vessels. Techniques were developed to account for the effect of the reflected excitation on the measured fluorescence emission signal. An equation was developed based on the Beer-Lambert-Bougher law to calculate the lubricant excess surface density from the measured fluorescence intensity. The lubricant surface density measurements suggest that the excess layer is pure lubricant. The resulting thickness of the non-adiabatic excess layer for a pure lubricant excess layer ranged from 0.04 mm to 0.06 mm depending on the heat flux.

The boiling heat transfer measurements that were simultaneously taken with the fluorescence measurements show that the R123/York-C™ (98.2/1.8) mixture exhibited a degradation for most all the heat fluxes that were tested. For heat fluxes between 28 kW/m^2 and 35 kW/m^2, the heat transfer may not have differed from the pure refrigerant. Overall, the R123/York-C™ (98.2/1.8) mixture heat flux from 20 kW/m2 to 54 kW/m2 was on average 12 % less than that of pure R123.

ACKNOWLEDGEMENTS

This work was jointly funded by NIST and the U.S. Department of Energy (project no. DE-01-95CE23808.000 modification #A004) under Project Manager Esher Kweller. Thanks go to the following NIST personnel for their constructive criticism of the first draft of the manuscript: Dr. P. Domanski, Dr. V. Payne, and Dr. D. Ross. The author would also like to express appreciation to Mr. G. Glaeser, Mr. V. Basumallick, and Mr. C. Henry of the NIST Building Environment Division for data collection. Furthermore, the author extends appreciation to Dr. W. Guthrie and Mr. A. Heckert of the NIST Statistical Engineering Division for their consultations on the uncertainty analysis. Special thanks goes to Dr. T. Vorburger of the NIST Precision Engineering Division for making the roughness measurements of the crosshatch surface. Thanks go to the following NIST personnel: Dr. T. Bruno, Mr. D. Plusquellic, and Dr. G. Fraser for consultations on fluorescence and assistance with the measurement of the absorption spectrum for lubricant. Thanks also goes to Dr. D. Ross of the NIST Process Measurements Division for discussions on excess surface density. The York-C™ lubricant that was donated by Mr. K. Starner and York International is much appreciated. Mr. F. Brogna and Mr. R. Collins of Optical Technology Devices, Inc. designed the modification for the spectrofluorometer to accept the bifurcated optical bundle and were essential in discussions concerning its operation.

NOMENCLATURE

English Symbols

A	absorbance
c	concentration, mol/m^3
C	regression constants in eq 1
F	fluorescence intensity
F_c	fluorescence intensity from calibration (eq 6)
F_m	fluorescence intensity measured from boiling surface
I_o	incident intensity, V
I_t	transmitted intensity, V
k	thermal conductivity, W/m·K
l	path length, m
l_e	thickness of excess layer, m
L_y	length of test surface, m
M_L	molar mass of lubricant, kg/mol
q''	average wall heat flux, W/m^2
R_a	average roughness, m
Ra_L	Rayleigh number based on A_s/p (Fig. 10)
T	temperature, K
T_w	temperature at roughened surface, K
S_m	mean peak spacing parameter, m
U	expanded uncertainty
u_i	standard uncertainty
v	volts, V
x	test surface coordinate in Fig. 4, m
x_m	mass fraction of lubricant
X	model terms given in Table 1
y	test surface coordinate in Fig. 4, m

Greek symbols

ΔT	wall superheat: T_w - T_s, K
ε	extinction coefficient
Γ	surface excess density, kg/m^2
λ	wavelength, m
Φ	quantum efficiency of fluorescence
ρ	mass density of liquid, kg/m^3

English Subscripts

b	bulk
e	excess layer
L	lubricant
m	emission, mixture
p	pure R123
q"	heat flux
s	saturated state, solid surface

Tw wall temperature
x excitation

Greek Subscripts

λ wavelength

Superscripts
- average

REFERENCES

Adamson, A. W., 1967, Physical Chemistry of Surfaces, Interscience Publ., New York, 2nd Ed., p. 353.

Amadeo, J. P., Rosén C., and Pasby, T. L., 1971, Fluorescence Spectroscopy An Introduction for Biology and Medicine, Marcel Dekker, Inc., New York, p. 153.

Baustian, J. J., Pate, M. B., and Bergles, A. E., 1988a, "Measuring the Concentration of a Flowing Oil-Refrigerant Mixture with an Acoustic Velocity Sensor," ASHRAE Trans., Vol. 94, No. 2, pp. 602-615.

Baustian, J. J., Pate, M. B., and Bergles, A. E., 1988b, "Measuring the Concentration of a Flowing Oil-Refrigerant Mixture with a Bypass Vicometer," ASHRAE Trans., Vol. 94, No. 2, pp. 588-594.

Baustian, J. J., Pate, M. B., and Bergles, A. E., 1988c, "Measuring the Concentration of a Flowing Oil-Refrigerant Mixture with a Vibrating U-Tube Densimeter," ASHRAE Trans., Vol. 94, No. 2, pp. 571-587.

Bayani, A., Thome, J. R., and D. Favrat, 1995, "Online Measurement of Oil Concentrations of R-134a/Oil Mixtures with a Density Flowmeter," HVAC&R Research, Vol. 1, No. 3, pp. 232-241.

Eckert, E. R. G., and Goldstein, R. J., 1976, Measurements in Heat Transfer, Hemisphere, Washington, 2nd ed., pp. 9-11.

Guilbault, G. G., 1967, Fluorescence: Theory, Instrumentation, and Practice, Edward Arnold LTD., London, pp. 91-95.

Incropera, F. P., and DeWitt, D. P., 1985, Fundamentals of Heat and Mass Transfer, 2nd ed., John Wiley & Sons, New York.

Kayser, R. F., Moldover, M. R., and Schmidt, J. W., 1986, "What Controls the Thickness of Wetting Layers?," J. Chem. Soc., Faraday Trans. 2, Vol. 82, pp. 1701-1719.

Kedzierski, M. A., 2001, "The Effect of Lubricant Concentration, Miscibility and Viscosity on R134a Pool Boiling," Int. J. Refrigeration, Vol. 24, No. 4.

Kedzierski, M. A., 1999, "Enhancement of R123 Pool Boiling by the Addition of N-Hexane," Journal of Enhanced Heat Transfer, Vol. 6, No. 4, pp. 89-100.

Kedzierski, M. A., Bruno, T. J., and O'Neil, M. B., 1998,"A New Insitu Technique for Measuring the Concentration of Lubricant on a Boiling Heat Transfer Surface," NISTIR 6110, U.S. Department of Commerce, Washington, D.C.

Kedzierski, M. A., 1995, "Calorimetric and Visual Measurements of R123 Pool Boiling on Four Enhanced Surfaces," NISTIR 5732, U.S. Department of Commerce, Washington.

Kedzierski, M. A., and Worthington, J. L. III, 1993, "Design and Machining of Copper Specimens with Micro Holes for Accurate Heat Transfer Measurements," Experimental Heat Transfer, Vol. 6. pp. 329-344.

Kedzierski, M. A., 1993, "Simultaneous Visual and Calorimetric Measurements of R11, R123, and R123/Alkylbenzene Nucleate Flow Boiling," Heat Transfer with Alternative Refrigerants, HTD-Vol. 243, H.J. Sauer, Jr., and T.H. Kuehn, Eds., ASME, New York, pp. 27-33.

Kedzierski, M. A., and Kaul, M. P., 1993, "Horizontal Nucleate Flow Boiling Heat Transfer Coefficient Measurements and Visual Observations for R12, R134a, and R134a/ Ester Lubricant Mixtures," *The 6th International Symposium on Transport Phenomena in Thermal Engineering, Seoul, Korea*, Vol. 1, pp. 111-116.

Marto, P. J. and Lepere, V. J., 1982, "Pool Boiling Heat Transfer From Enhanced Surfaces to Dielectric Fluids," ASME Journal of Heat Transfer, Vol. 104, pp. 292-299.

McBain, J. W., and Humphreys, C. W., 1932, "The Microtome Method of the Determination of the Absolute Amount of Adsorption," J. Chem. Phys., Vol. 36, pp. 300-311.

Meyer, J. J., and Saiz Jabardo, J. M., 1994, "An Ultrasonic Device for Measuring the Oil Concentration in Flowing Liquid Refrigerant," Int. J. of Refrigeration, Vol. 17, No. 7, pp. 481-486.

Miller, J. N., 1981, Volume Two Standards in Fluorescence Spectrometry, Chapman and Hall, London, pp. 44-67.

Morrison, G, and Ward, D. K., 1991, "Thermodynamic Properties of Two Alternative Refrigerants: 1,1-Dichloro-2,2,2-Trifluoroethane (R123) and 1,1,1,2-Tetrafluoroethane (R134a)," Fluid Phase Equilibria, Vol. 62, pp. 65-86.

Navarro de Andrade, E., Skowron, E., Goldschmidt, V. W., and Groll, E. A., 1999, "Oil Concentration in liquid refrigerants: in situ measurement," Int. J. of Refrigeration, Vol. 22, No. 6, pp. 499-508.

Reader, J, Corliss, C. H., Wiese, W. L., and Martin, G. A., 1980, "Wavelengths and Transition Probabilities of Atoms and Atomic Ions", NSRDS-National Bureau of Standards #68, U.S. Department of Commerce, Washington.

Rosen, M. J., 1978, Surfactants and Interfacial Phenomena, John Wiley & Sons, New York, p. 57.

Siu, M. C. I., Carroll, W. L., and Watson, T. W., 1976, "Thermal Conductivity and Electrical Resistivity of Six Copper-Base Alloys," NBSIR 76-1003, U.S. Department of Commerce, Washington.

Stephan, K., 1963, "Influence of Oil on Heat Transfer of Boiling Refrigerant 12 and Refrigerant 22," XI Int. Congr. of Refrigeration, Vol. 1, pp. 369-380.

Suzuki, S., Fujisawa, Y., Nakazawa, S., and Matsuoka, M., 1993, "Measuring Method of Oil Circulation Ratio Using Light Absorption," ASHRAE Trans., Vol. 99, No. 1, pp. 413-421.

Vorburger, T. V., and Raja, J., 1990, "Surface Finish Metrology Tutorial," NISTIR 89-4088, U.S. Department of Commerce, Washington.

Webb, R.L., and Pais, C., 1992, "Nucleate Pool Boiling Data for Five Refrigerants on Plain, Integral-fin and Enhanced Tube Geometries," Int. J. Heat Mass Transfer, Vol. 35, No. 8, pp. 1893-1904.

Table 1 Conduction model choice

X_0= constant (all models) X_1= x X_2= y X_3= xy X_4=x^2-y^2 X_5= y(3x^2-y^2) X_6= x(3y^2-x^2) X_7= x^4+y^4-6(x^2)y^2 X_8= yx^3-xy^3	
Fluid	Most frequent models
R123 (File: 123pln.dat)	X_1,X_2,X_4,X_5 (124 of 185) 67 % X_1,X_2,X_4,X_6 (21 of 185) 11 %
R123 (File: 123pln2.dat)	X_1,X_2,X_4,X_6 (24 of 68) 37 % X_1,X_2,X_4,X_5 (23 of 68) 31 % X_1,X_2,X_4 (11 of 68) 16 %
R123/ York-C™ (98.2/1.8)	X_1,X_2,X_4,X_5 (49 of 144) 34 % X_1,X_2,X_4,X_8 (20 of 144) 14 % X_1,X_3,X_4,X_6 (15 of 144) 10 % X_1,X_2,X_4,X_6,X_8 (10 of 144) 10 %

Table 2 Pool boiling data

Pure R123

File: 123pln.dat

ΔT_s (K)	q'' (W/m^2)
15.49	62727.4
15.28	56954.8
15.24	57668.7
15.23	57460.2
14.56	38710.8
14.44	38294.3
15.81	54260.4
15.78	53939.6
14.60	35042.9
16.32	80003.1
16.30	78769.2
16.29	79460.0
16.02	71899.3
15.98	69554.5
16.49	72993.7
16.46	72643.8
16.42	72675.9
15.89	54797.7
15.84	56102.0
15.81	55572.0
15.19	43239.0
15.18	43526.6
15.17	43517.8
14.67	32353.8
16.74	79528.5
16.71	80517.4
16.70	80512.9
16.04	64927.8
16.04	64927.8
16.02	64925.2
15.93	62669.1
15.70	56762.8
15.68	56637.9
15.67	56155.6
15.22	41141.3
15.23	40735.1
15.18	40308.8
15.19	40288.1
14.65	28870.8
14.60	28653.5
14.55	28693.8
13.68	23503.5
13.70	23438.1
13.66	23336.4
11.39	16554.2
11.34	16672.0
16.73	74572.9
16.66	74619.1
16.66	74482.7
16.20	64724.5
16.19	64132.3
16.12	62425.3
15.76	53983.2
15.73	55766.6
15.76	55732.6
15.25	40498.1
15.22	40227.9
15.14	41262.6
15.16	41050.0
13.34	22602.7
13.37	22214.8
16.80	70666.9
16.80	71175.8
16.80	71422.4
16.60	66764.6
16.57	66745.7
16.54	66422.4
16.19	59449.5
16.20	60454.8
16.28	62287.7
15.76	56003.9
15.76	56178.4
16.84	68867.5
16.82	68859.8
16.81	68543.9
16.21	54598.7
16.17	54652.0
15.46	38126.7
15.40	38019.4
14.60	26402.6
14.73	27388.9
14.70	28595.2
13.45	22591.9
13.64	24113.0
10.84	15998.8
10.84	16017.3
10.80	15729.4
16.87	76664.8
16.48	64065.8
16.38	63409.9
16.32	61380.7
15.61	41301.9
15.53	40856.3
15.47	39894.9
15.33	37529.0
15.29	37086.1
15.27	37100.9
14.39	27473.9
14.41	26661.8
14.32	26799.7
16.71	72964.4
16.70	72885.7
16.68	72797.2
16.12	52678.6
16.11	52610.4
16.09	52469.4
15.20	31624.8
15.20	31330.2
15.38	35111.4
12.98	20044.9
12.89	19889.1
12.88	19934.9
16.79	73022.5
16.75	72718.0
16.73	72571.4
16.29	61681.7
16.31	61667.8
16.14	61906.6
15.31	35091.6
15.40	35886.4
17.12	75360.3
17.05	71905.2
17.05	73114.3
16.69	68294.1
16.70	68134.3
16.71	68015.0
16.29	48216.3
16.10	49173.0
16.10	48969.8
15.73	38426.1
15.72	38323.8
15.70	38263.2
15.57	35833.7
15.59	36460.0
15.57	36671.3
15.42	33108.1
15.40	32847.8
15.38	32928.3
17.05	71905.2
17.05	73114.3
16.69	68294.1
16.70	68134.3
16.71	68015.0
16.29	48216.3
16.10	49173.0
16.10	48969.8
15.73	38426.1
15.72	38323.8
15.70	38263.2
15.57	35833.7

15.59	36460.0
15.57	36671.3
16.97	73460.4
16.97	74198.4
17.02	75802.9
15.67	35238.8
15.59	34477.1
15.60	34730.0
15.12	32468.4
15.08	32737.2
15.08	32414.7
12.41	18818.6
12.40	18761.6

Pure R123
File: 123pln2.dat

ΔT_s (K)	q'' (W/m^2)
20.96	51516.8
20.95	51381.9
20.91	51358.2
19.85	36938.9
19.81	36818.1
19.77	36634.6
15.83	27062.6
15.90	27305.7
15.87	27065.8
13.97	25444.9
13.93	25765.2
20.94	49607.1
21.15	58049.7
20.93	49971.5
20.82	44608.1
20.83	44912.0
20.84	45247.8
20.65	39145.3
20.62	38866.3
20.56	38665.1
18.69	32828.1
18.70	32771.1
18.73	32615.6
13.87	23043.1
13.85	22883.7
21.02	54003.9
21.04	55865.2
21.03	55887.4
20.70	40925.4
20.66	39443.3
20.65	39379.1
20.59	38513.3
20.68	39381.5

20.70	39928.3
19.33	34477.3
19.17	34690.7
19.43	35237.4
16.91	29980.1
16.96	30330.8
21.04	51875.8
21.05	51925.5
21.06	51638.5
20.80	41780.6
20.82	41812.3
20.77	41833.2
16.76	28323.4
16.85	28288.0
16.84	28389.8
11.54	18828.5
11.66	19059.0
21.08	52080.7
21.10	52442.5
21.09	52312.6
14.46	26300.0
14.66	26415.0
14.59	26401.7
14.59	26401.7
12.70	21604.8
12.66	21369.8
12.73	21939.9
21.15	58049.7
20.93	49971.5
21.07	51277.6
21.07	51287.1
21.09	51249.8
19.95	34261.8
20.02	34650.3
20.02	34587.9
15.96	27103.5

R123/York-C™
(98.2/1.8)
File: R123YC2.dat

ΔT_s (K)	q'' (W/m^2)
22.21	53944.3
22.17	53724.3
22.13	53503.6
21.84	45824.1
21.84	45824.1
21.84	44962.6
21.82	44882.4
21.29	40681.3
21.27	40646.1
21.17	40465.1
20.47	36648.0

20.51	36989.7
20.51	36959.1
19.59	33463.6
19.52	33461.1
19.54	33309.4
18.21	29964.9
22.22	46329.8
22.25	46543.4
22.26	46574.8
22.07	44266.8
22.07	44400.9
22.06	44249.4
21.41	39123.7
21.38	39218.5
21.36	38660.1
20.29	34461.4
20.27	35017.7
20.31	35381.5
19.04	31524.5
18.76	30930.4
18.68	31167.5
18.60	31290.2
18.77	30820.1
18.87	31150.7
17.15	27364.6
17.07	27110.5
16.99	27059.2
16.07	25608.0
22.22	46329.8
22.25	46543.4
22.26	46574.8
22.07	44266.8
22.07	44400.9
22.06	44249.4
21.41	39123.7
21.38	39218.5
21.36	38660.1
20.29	34461.4
20.27	35017.7
20.31	35381.5
19.04	31524.5
18.76	30930.4
18.68	31167.5
18.60	31290.2
18.77	30820.1
18.87	31150.7
17.15	27364.6
17.07	27110.5
16.99	27059.2
16.07	25608.0
16.22	26126.8
15.81	25549.5

14.67	23160.5
14.54	23005.5
14.50	22920.4
13.33	20168.2
13.53	20909.9
13.56	20872.0
12.54	19086.0
12.56	18976.1
12.56	19115.5
10.97	15988.8
22.22	45328.3
22.22	45267.3
22.21	45138.2
21.56	39448.3
18.68	31167.5
21.63	39696.5
20.18	34127.3
20.19	34631.7
20.17	34638.3
18.25	29233.2
18.20	29657.6
18.32	33383.2
16.15	28950.0
16.08	28878.1
16.04	28911.9
14.55	26510.5
14.65	26508.9
14.78	27292.9
13.52	24708.1
13.56	24766.4
22.21	53639.9
22.18	53456.3
22.14	53356.4
21.79	47829.0
21.81	47728.2
21.88	47652.8
16.96	27460.3
16.93	27328.8
16.95	27438.7
14.58	23080.1
14.56	23169.2
14.71	24023.9
13.56	21483.1
13.81	21972.4
13.52	21289.9
12.49	19317.3
12.40	19192.5
12.41	19113.9
11.79	17877.8
12.03	18177.4
11.98	18298.7
10.85	15824.4

10.80	15859.0
10.73	15776.0
9.00	12770.6
9.02	12809.0
22.32	44777.5
22.30	53242.3
22.29	53351.8
22.05	46101.8
21.93	45764.2
21.90	45648.6
20.01	34290.3
19.79	33290.0
19.80	33047.9
18.13	29012.7
17.99	29152.6
17.97	29354.7
15.81	25212.3
15.75	25106.3
14.40	22293.3
14.31	22326.5
14.41	22447.5
13.24	20097.2
13.19	20084.9
13.24	20132.3
11.71	17266.6
11.67	17142.6
11.41	16606.5
11.01	16040.4
11.02	16113.3
11.03	16099.8
9.62	13410.0
9.55	13421.7
22.09	45478.6
21.90	48444.7
20.74	37165.2
19.89	34096.3
17.67	28425.1
17.38	27824.4
19.52	33438.9
17.66	27978.7
15.38	23847.4
15.67	25171.6
15.84	24800.1
13.84	21002.4
13.32	20179.8
13.30	20049.5

Table 3 Number of test days and data points

Fluid (% mass)	Number of days	Number of data points
R123 "break in data"	15	171
R123	6	69
R123/York-C™ (98.2/1.8)	6	144

Table 4 Constants for cubic boiling curve fits for plain copper surface

$\Delta T_s = A_0 + A_1 q'' + A_2 q''^2 + A_3 q''^3$

ΔT_s in Kelvin and q'' in W/m^2

Fluid		A_0	A_1	A_2	A_3
R123	$\Delta T_s \geq 13$ K	7.71421	4.17449×10^{-4}	-7.45117×10^{-9}	4.69661×10^{-14}
"break-in data "	$\Delta T_s \leq 13$ K	4.34389	-3.67068×10^{-4}	8.26988×10^{-8}	-2.14203×10^{-12}
R123	$\Delta T_s \geq 18$ K	-32.2044	3.20480×10^{-3}	-6.42276×10^{-8}	4.28317×10^{-13}
	$\Delta T_s \leq 18$ K	25.3837	-2.12686×10^{-3}	9.53098×10^{-8}	-1.11703×10^{-12}
R123a/York-C™ (99.5/0.5) $9 \text{ K} \leq \Delta T_s \leq 22.5$ K		2.98244	3.88456×10^{-4}	9.51211×10^{-9}	-1.92371×10^{-13}

Table 5 Residual standard deviation of ΔT_s from the mean

Fluid		U (K)
R123	$\Delta T_s \geq 13$ K	0.31
"break-in data "	$\Delta T_s \leq 13$ K	0.19
R123	$\Delta T_s \geq 18$ K	0.20
	$\Delta T_s \leq 18$ K	0.47
R123a/York-C™ (99.5/0.5) $9 \text{ K} \leq \Delta T_s \leq 22.5$ K		0.48

Table 6 Average magnitude of 95 % multi-use confidence interval for mean T_w-T_s(K)

Fluid		U (K)
R123	$\Delta T_s \geq 13$ K	0.17
"break-in data "	$\Delta T_s \leq 13$ K	0.28
R123	$\Delta T_s \geq 18$ K	0.20
	$\Delta T_s \leq 18$ K	0.67
R123a/York-C™ (99.5/0.5)	$\Delta T_s \geq 4.4$ K	0.24
	$\Delta T_s \leq 4.4$ K	

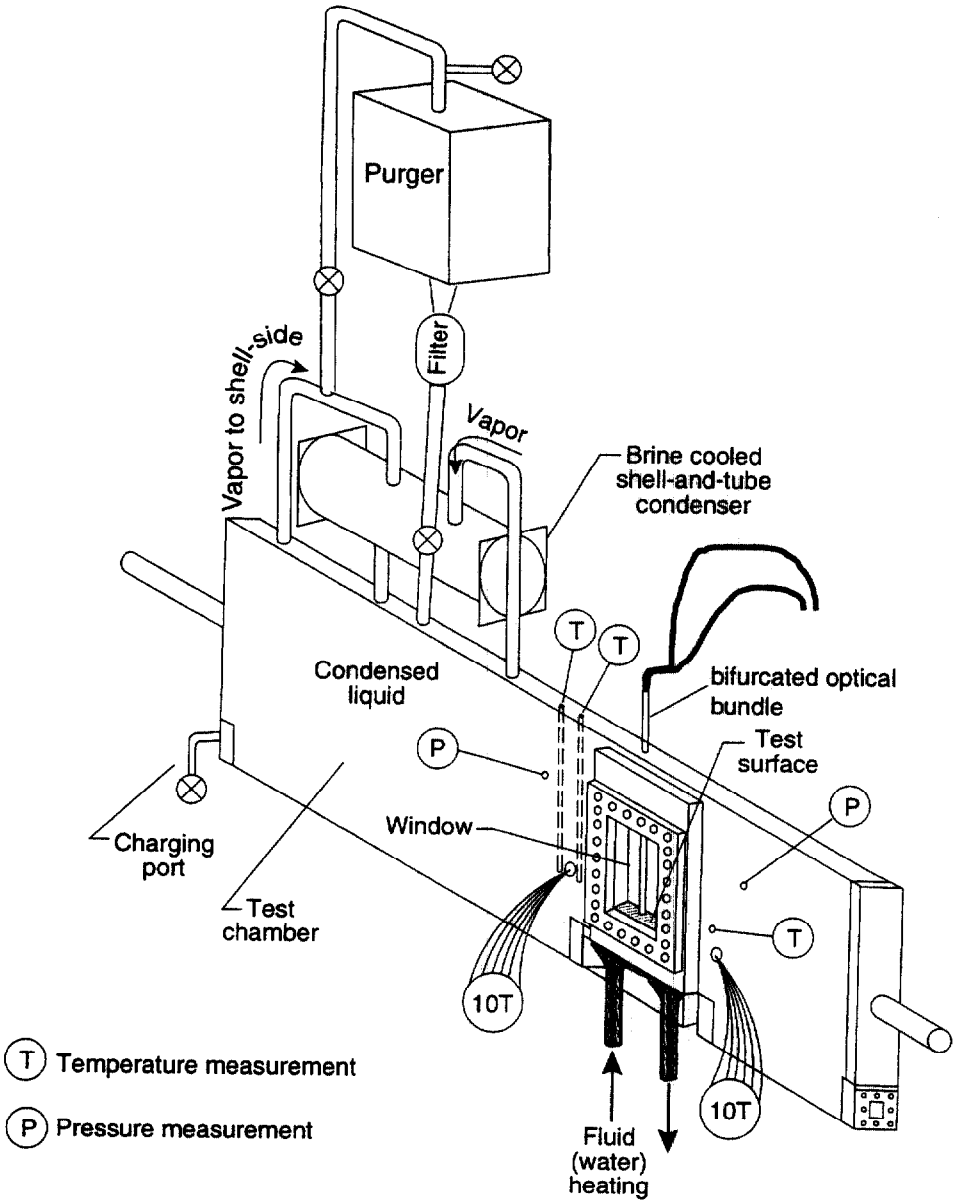

Fig. 1 Schematic of test apparatus

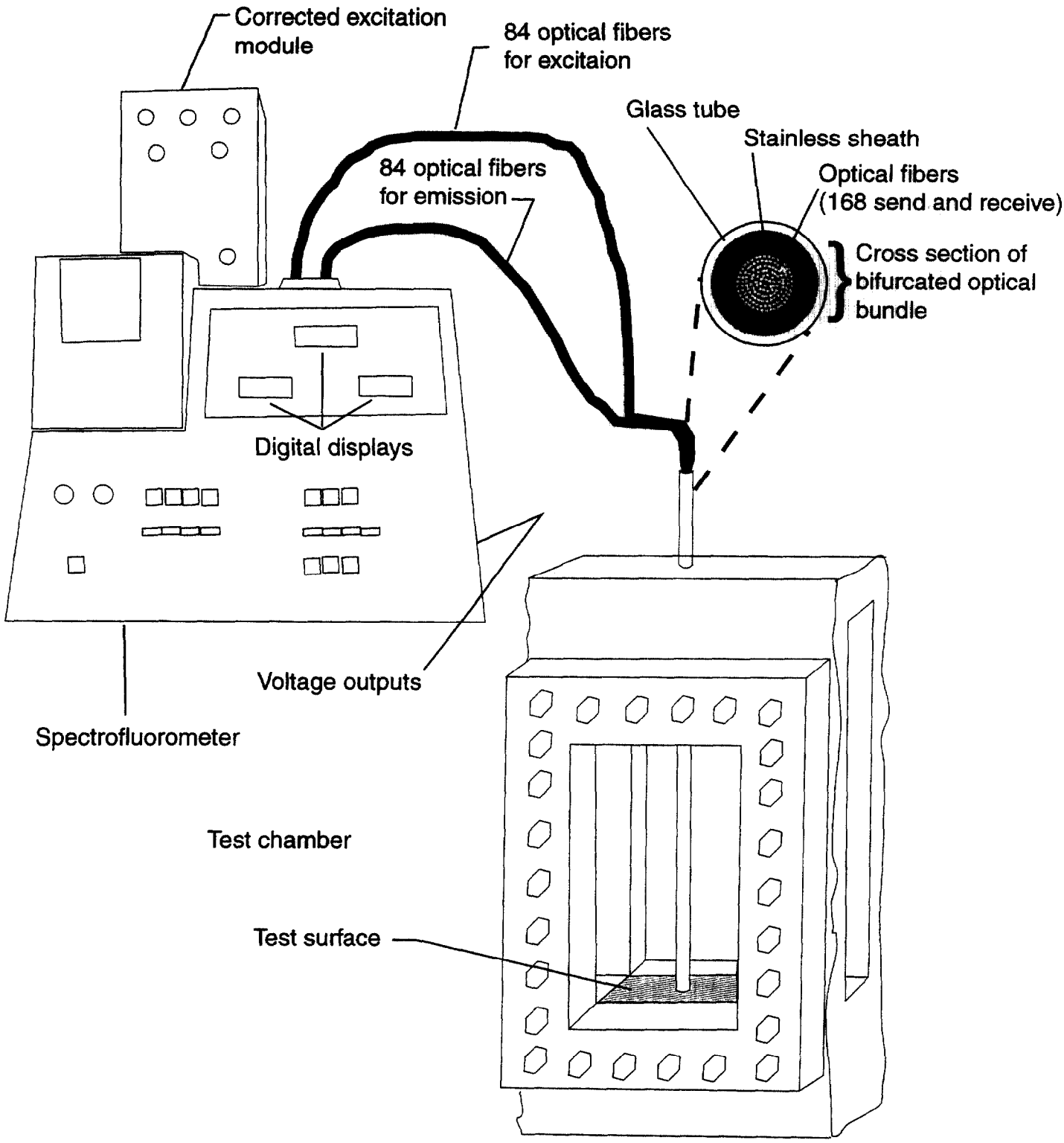

Fig. 2 Schematic of test chamber and spectrofluorometer

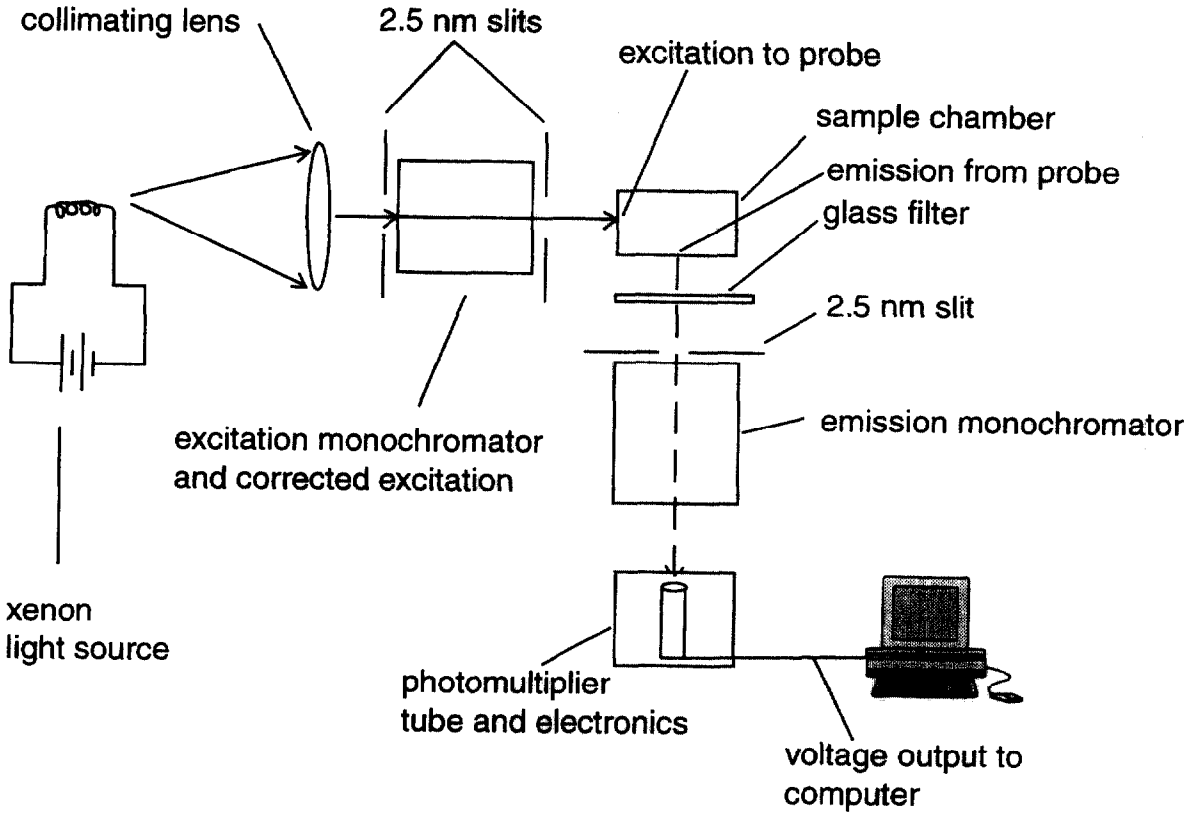

Fig. 3 Schematic of right angle spectrofluorometer

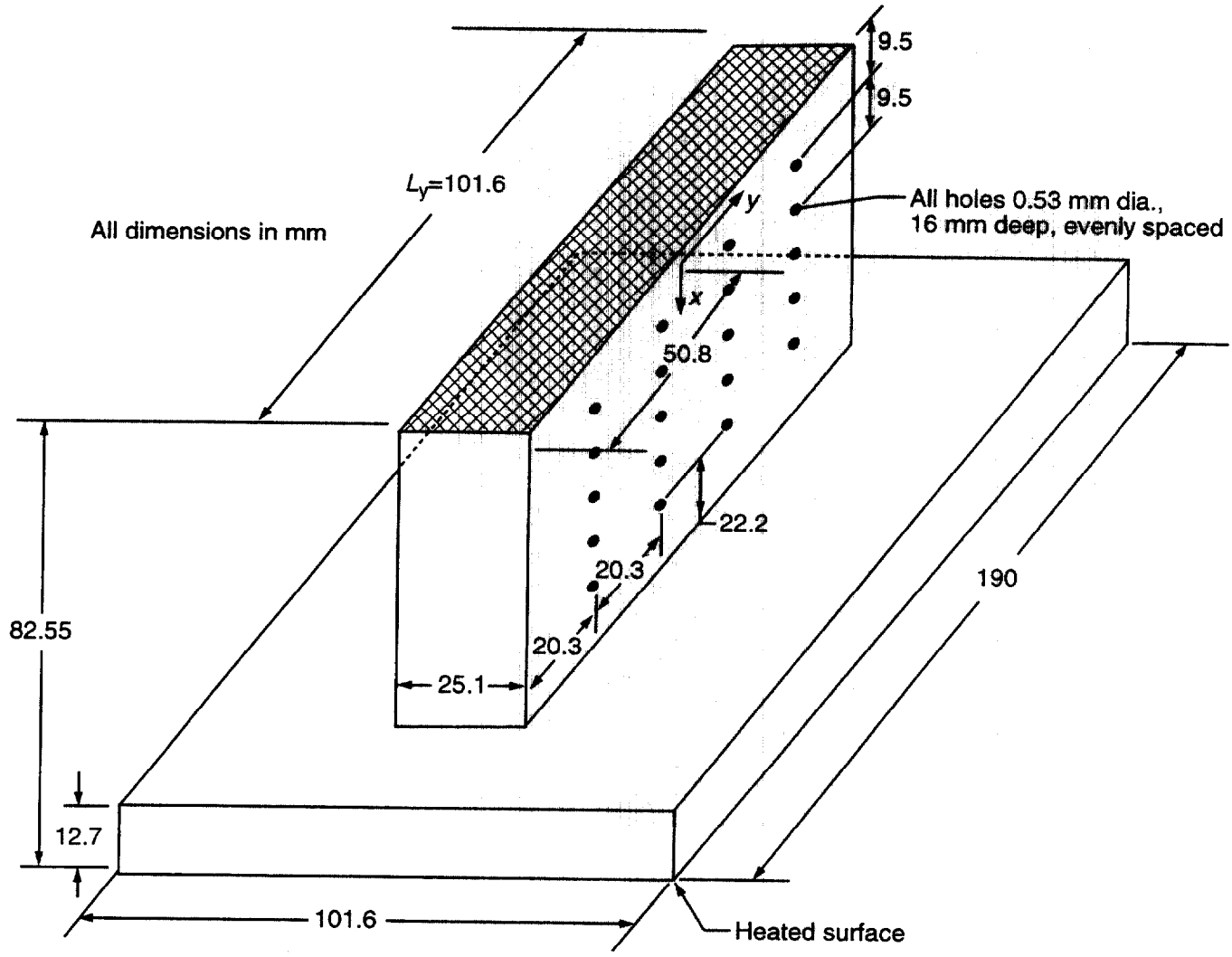

Fig. 4 OFHC copper flat test plate with cross-hatched surface and thermocouple coordinate system

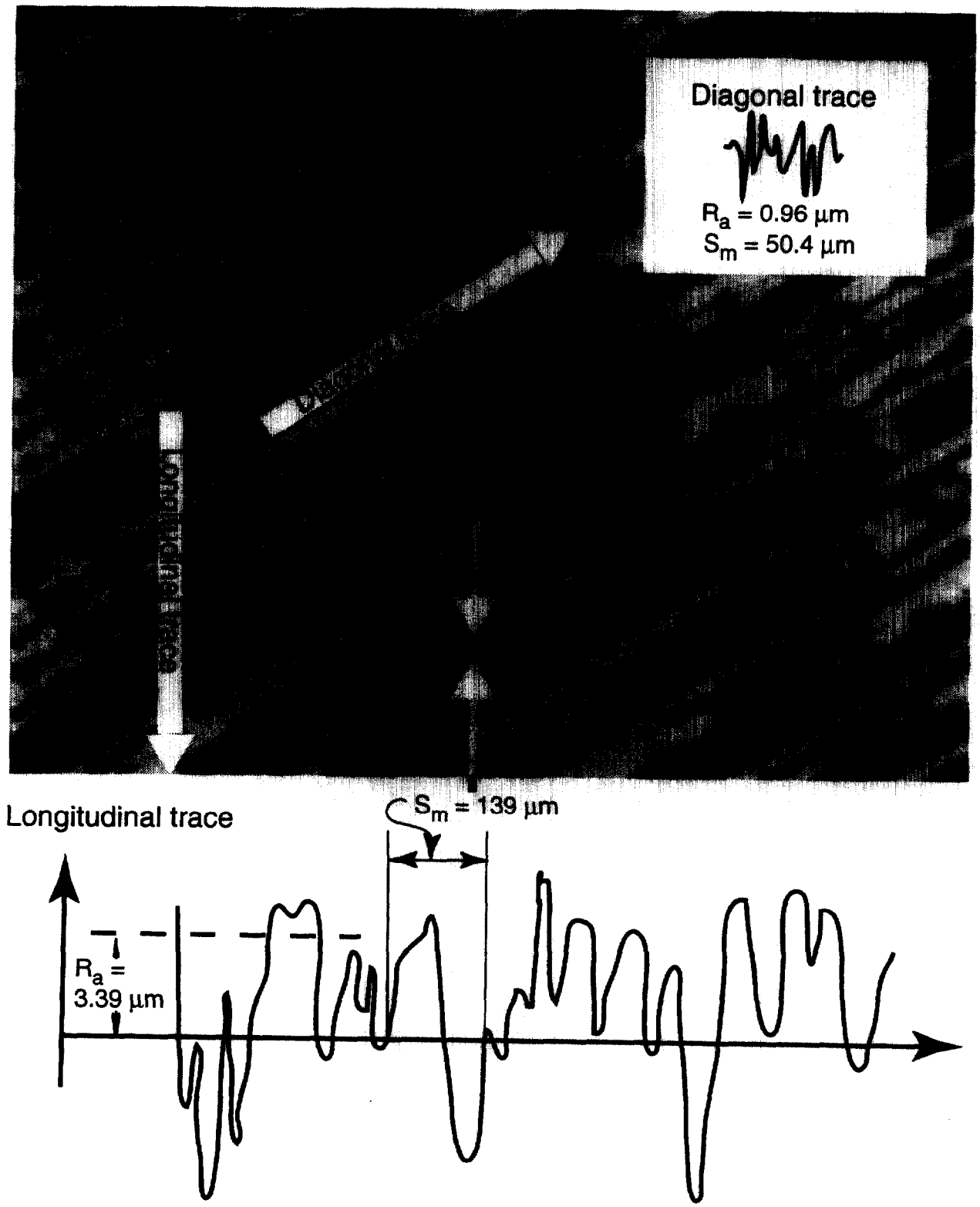

Fig. 5 Photograph of the OFHC test plate crosshatch surface with sample roughness traces

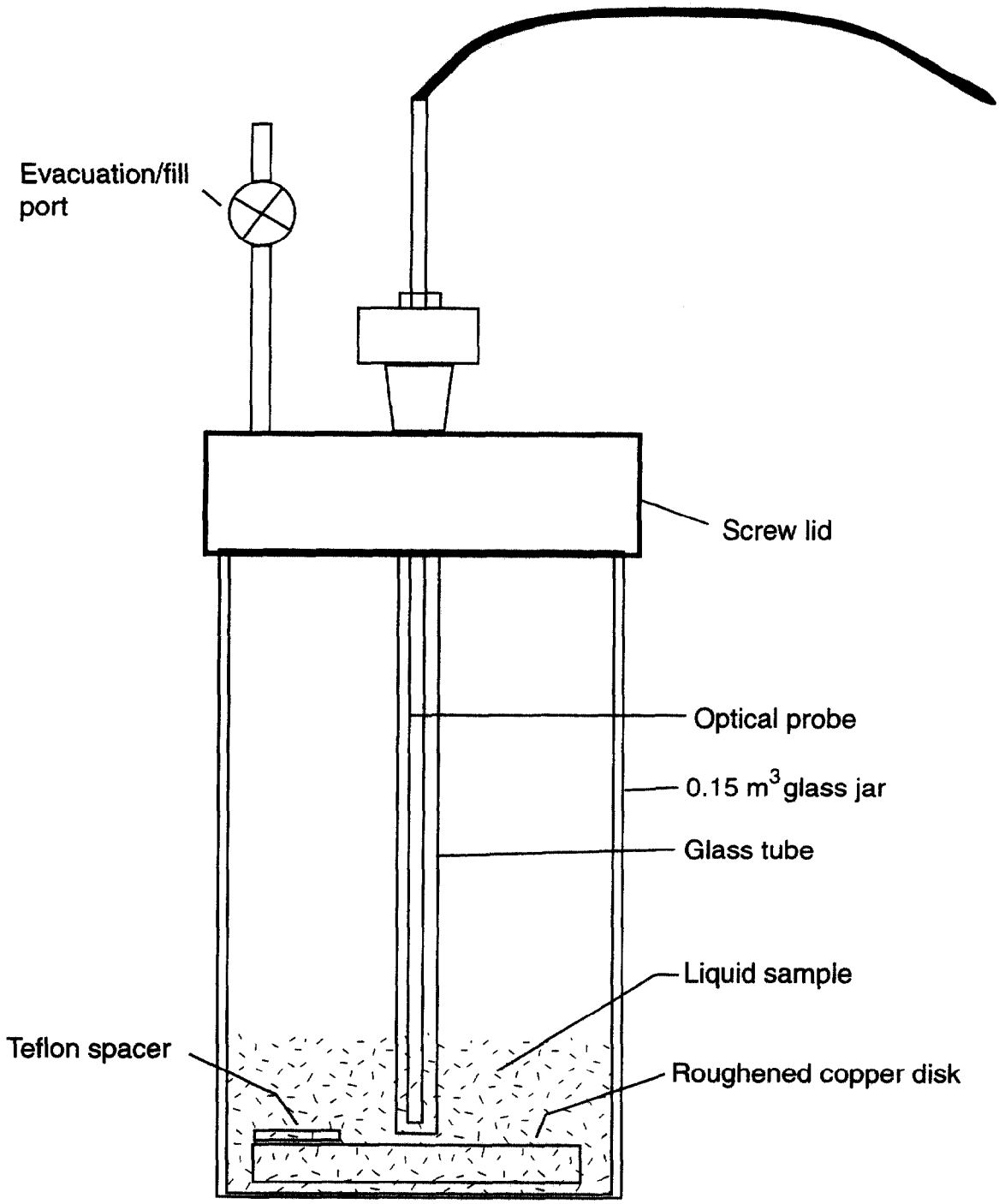

Fig. 6 Schematic of composition calibration jar

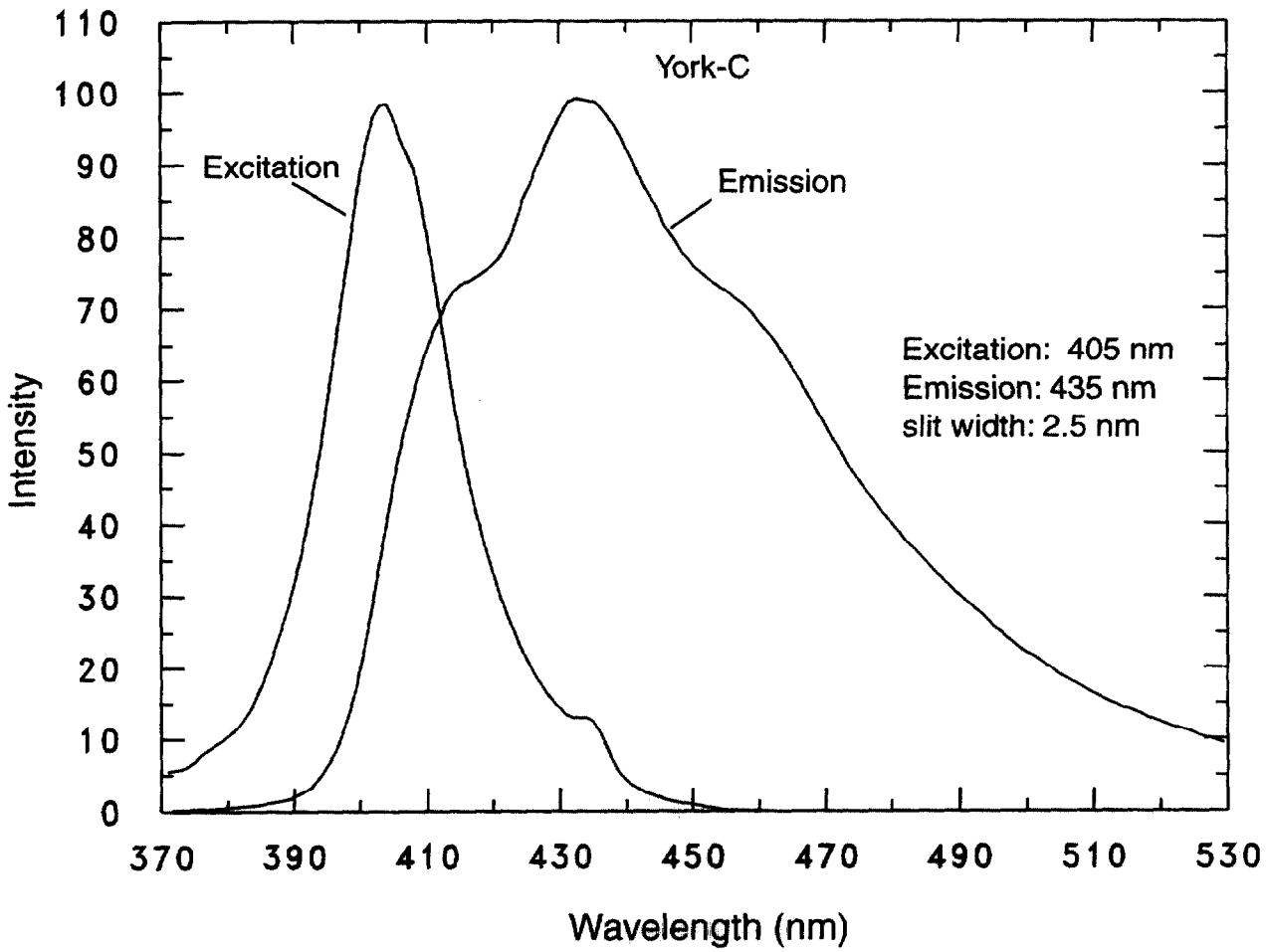

Fig. 7 Fluorescence spectra for pure York-C lubricant

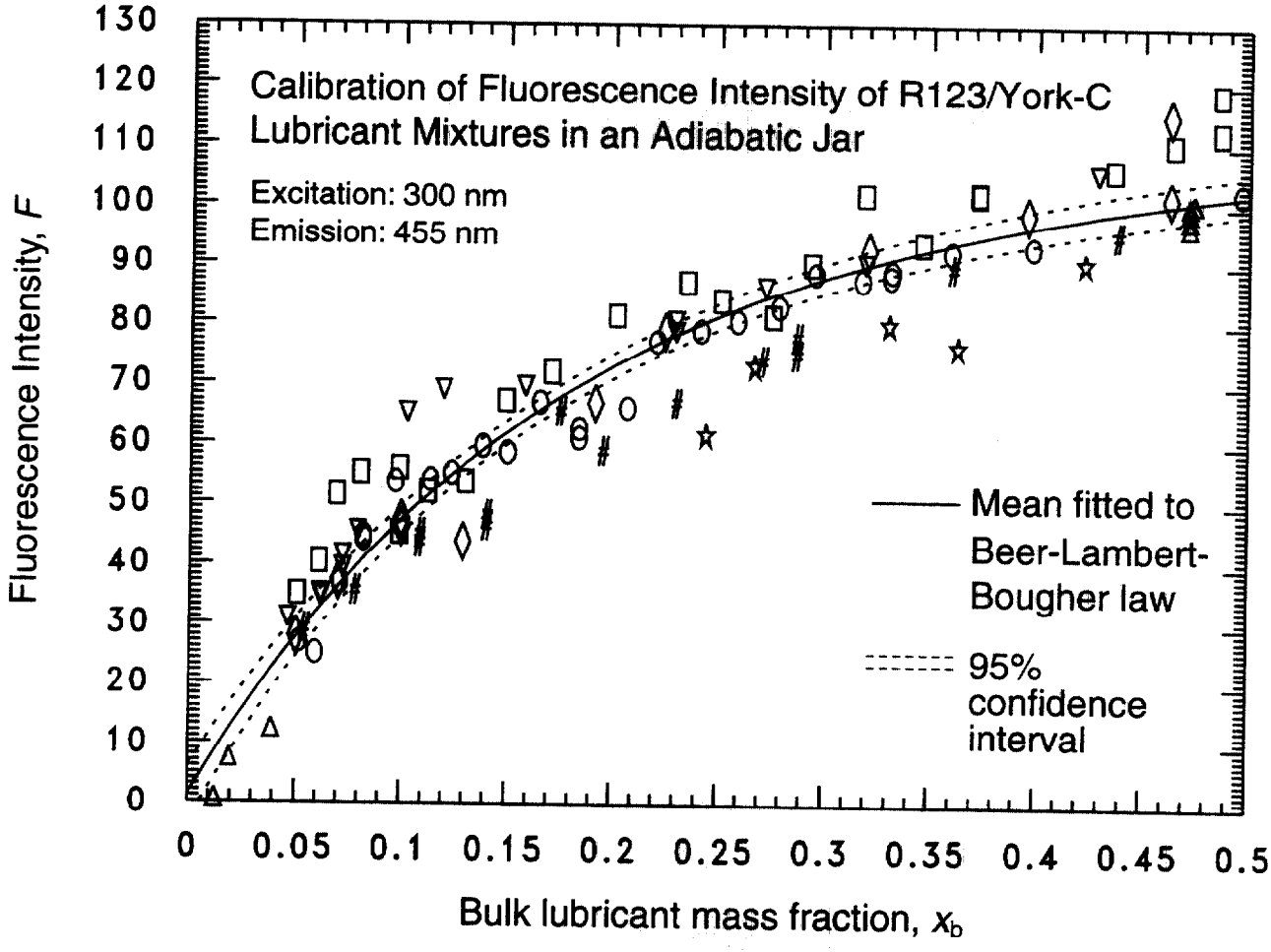

Fig. 8 Fluorescence calibration with F = 100 for R123/York-C™ (50/50) jar

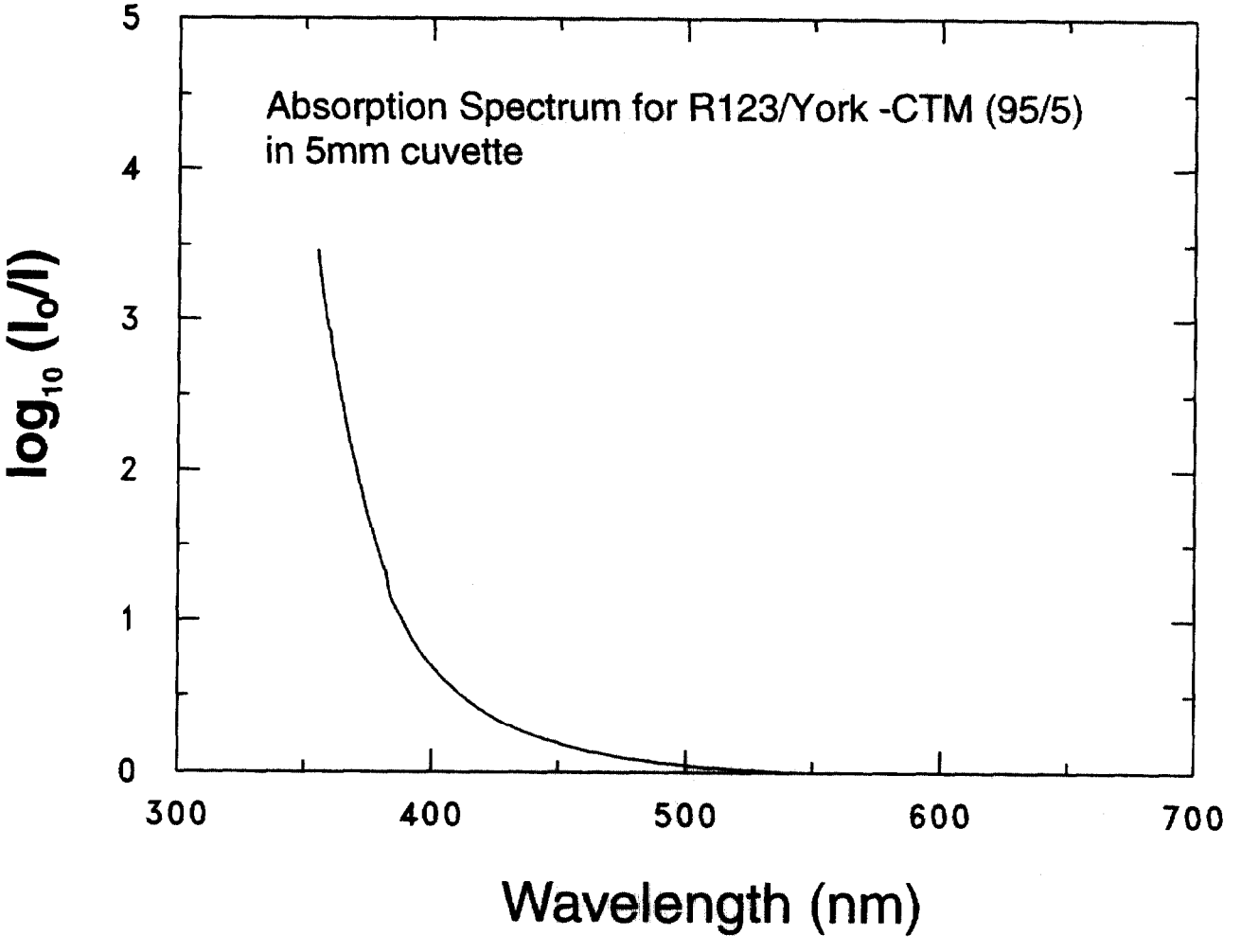

Fig. 9 Absorption Spectrum for R123/York-C™

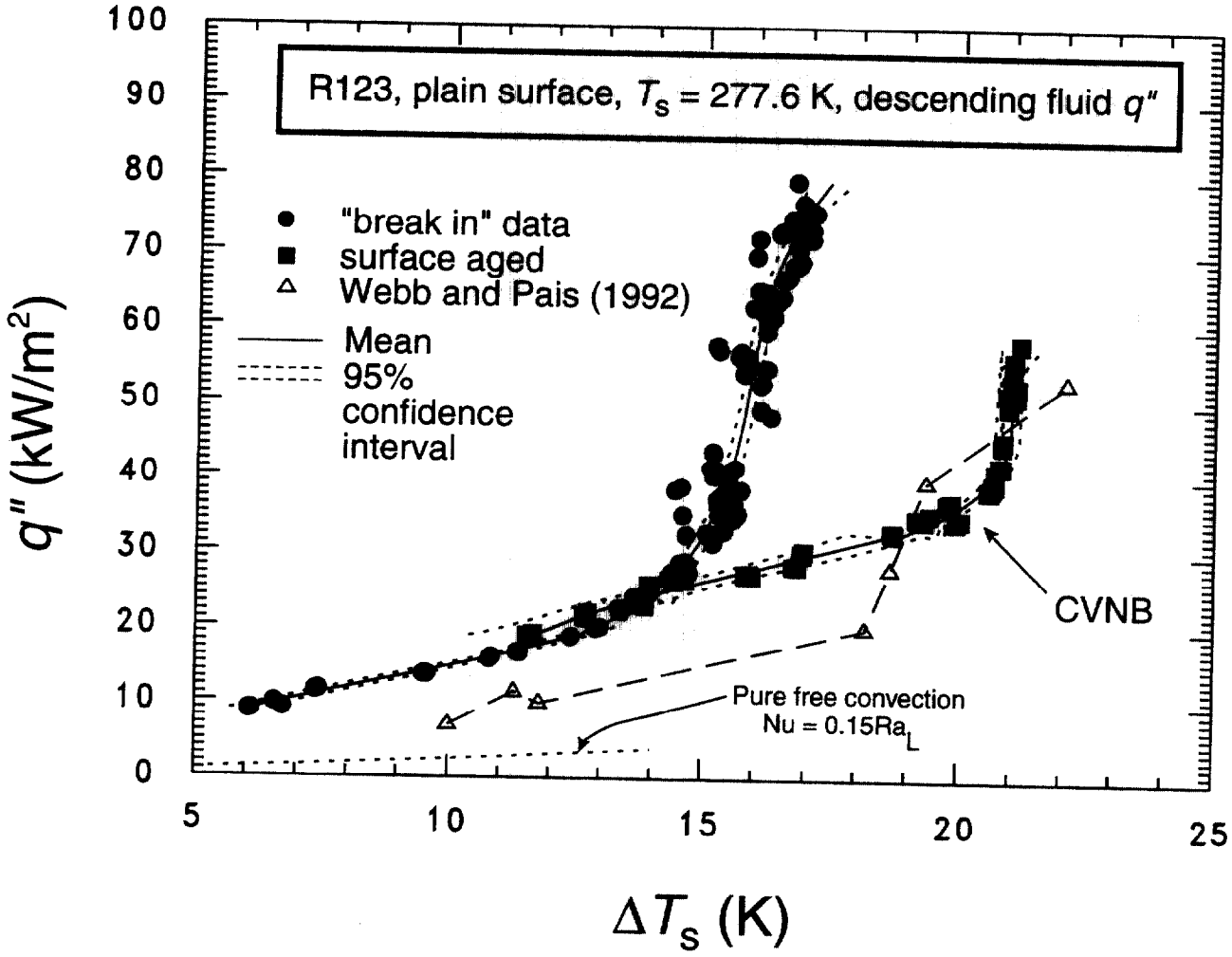

Fig. 10 Pure R123 boiling curves for plain surface

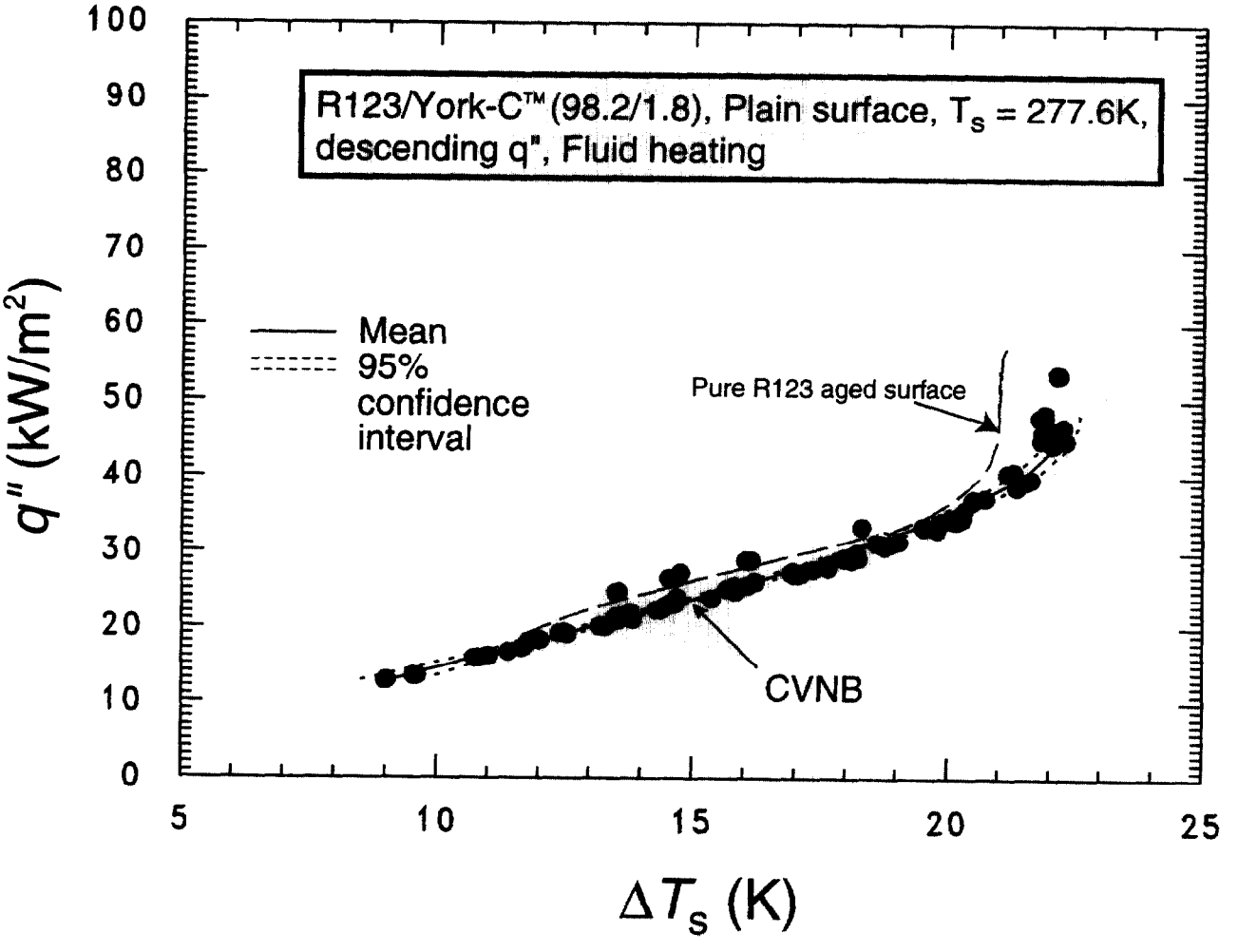

Fig. 11 R123/York-C™ (98.2/1.8) boiling curve for plain surface

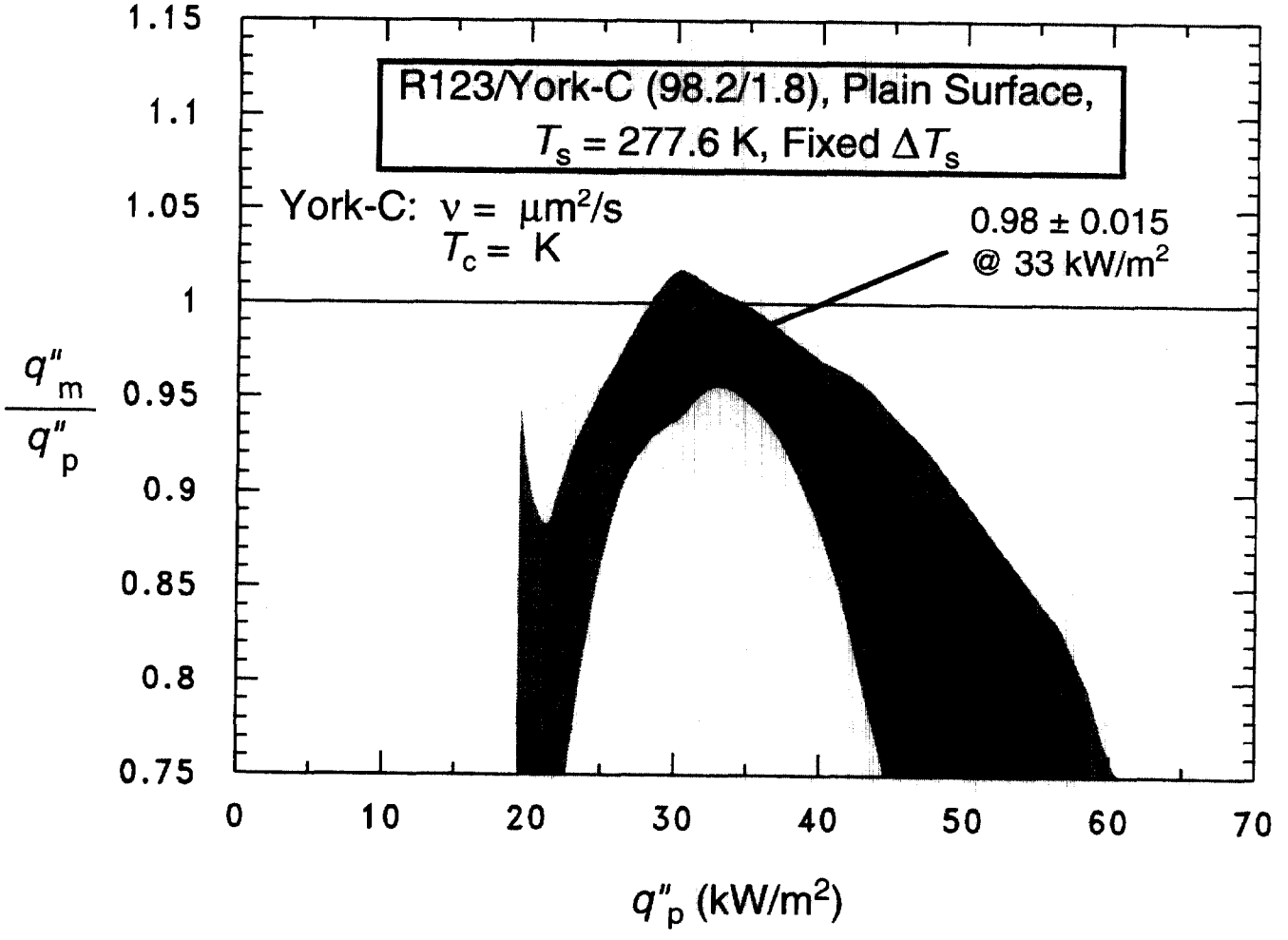

Fig. 12 R123/York-C™ (98.2/1.8) heat flux relative to that of pure R123

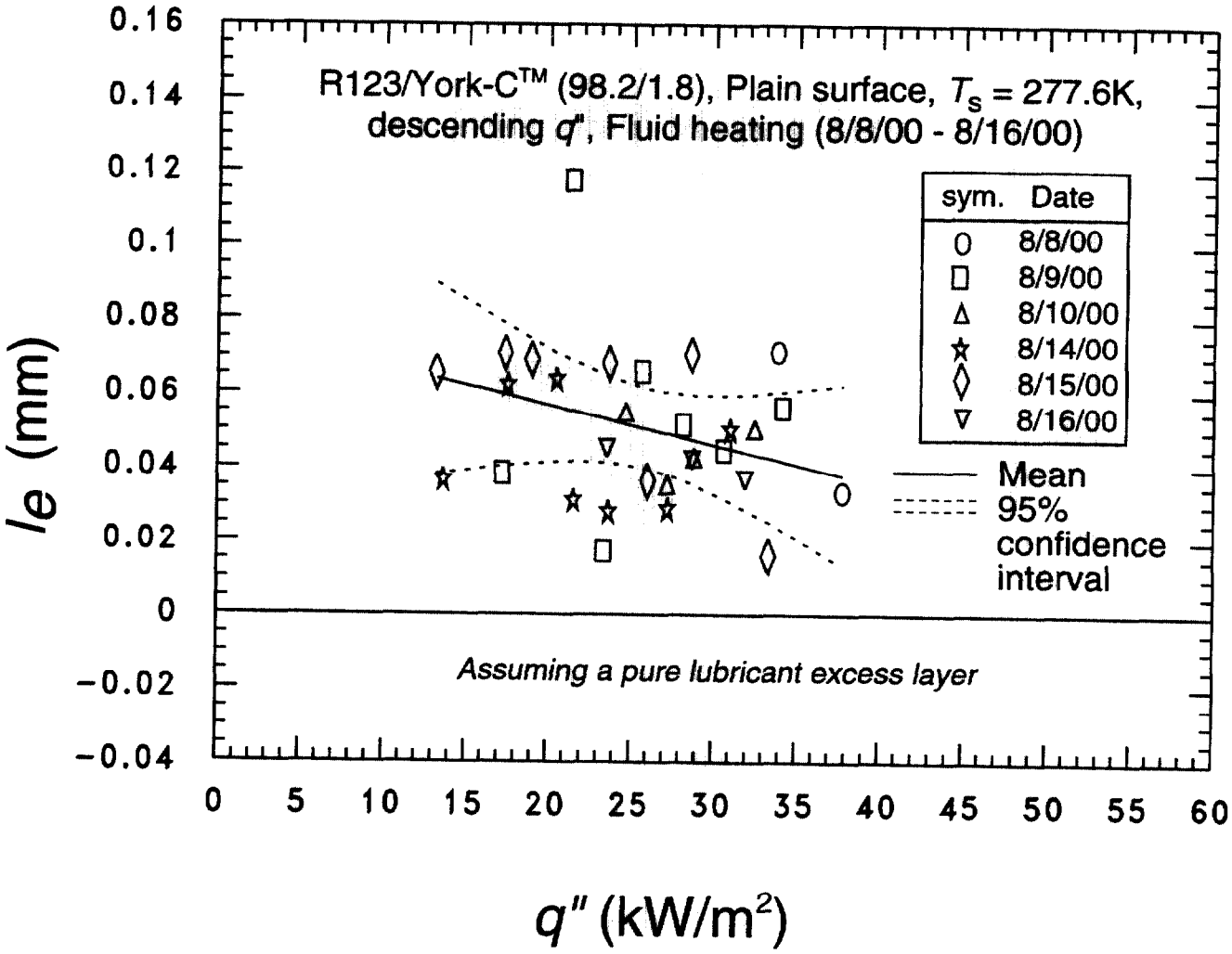

Fig. 13 Lubricant excess thickness for R123/York-C™ (98.2/1.8) as a function of heat flux

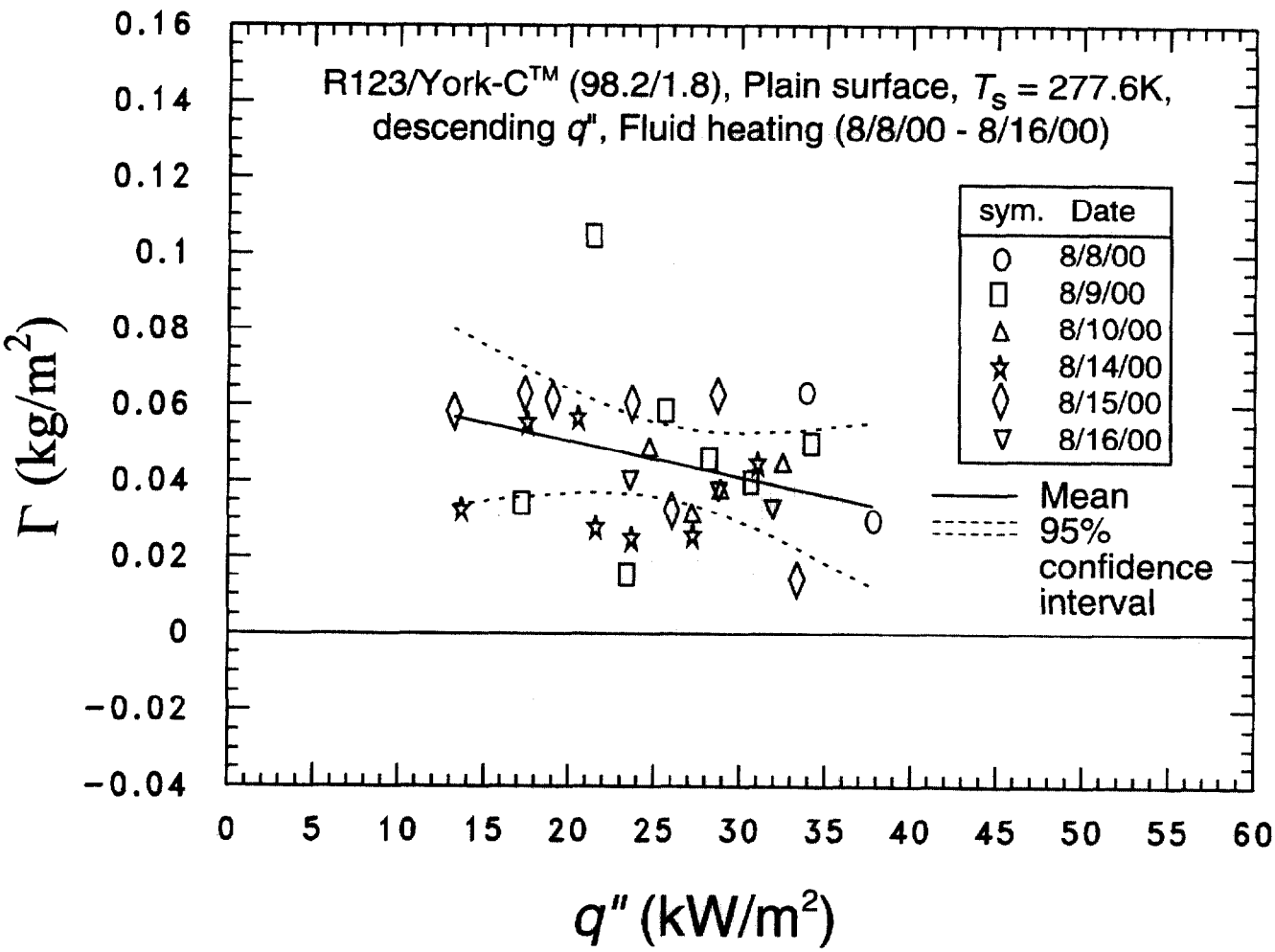

Fig. 14 Lubricant excess surface density for R123/York-C™ (98.2/1.8) as a function of heat flux

APPENDIX A

Figure A.1 shows the relative (percent) uncertainty of the heat flux ($U_{q"}$) as a function of the heat flux. Figure A.2 shows the uncertainty of the wall temperature as a function of heat flux. The uncertainties shown in Figs. A.1 and A.2 are "within-run uncertainties." These do not include the uncertainties due to "between-run uncertainties" or differences observed between tests taken on different days. The "within-run uncertainties" include only the random effects and uncertainties evident from one particular test. All other uncertainties reported here are "between-run uncertainties" which include all random effects such as surface past history or seeding. "Within-run uncertainties" are given only in Figs. A.1 and A.2.

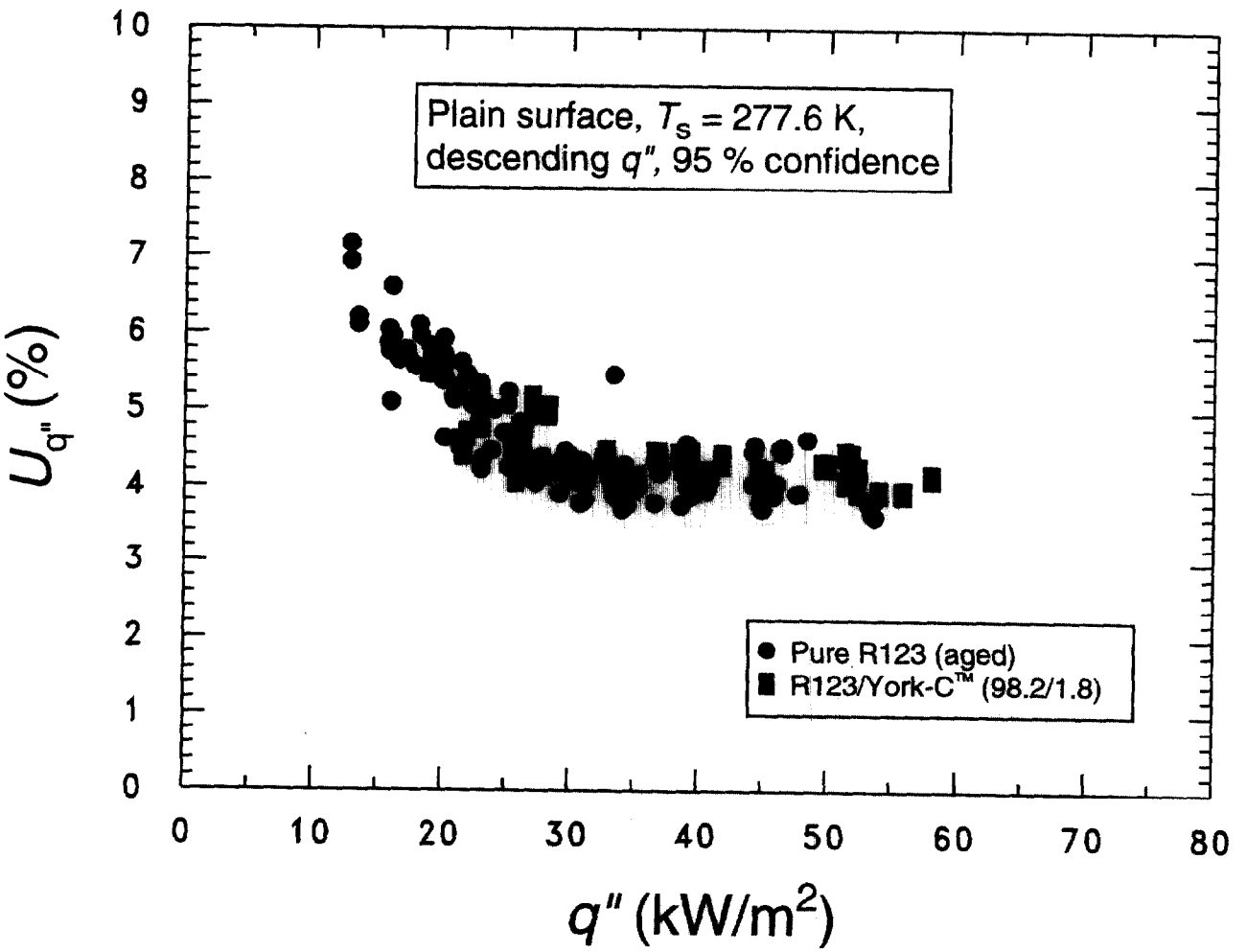

Fig. A.1 Uncertainty in the heat flux at surface for 95% confidence

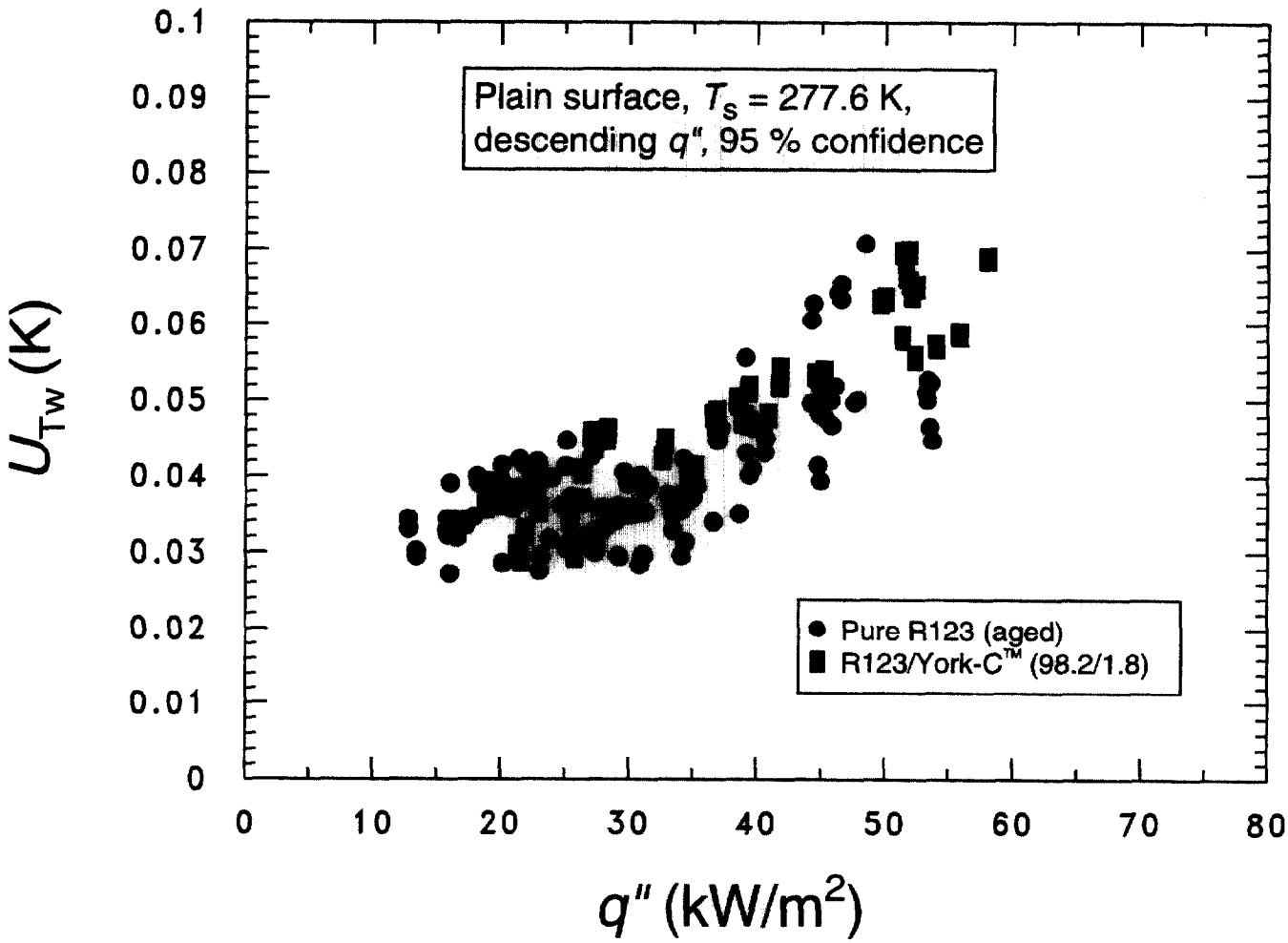

Fig. A.2 Uncertainty in the temperature of the surface for 95 % confidence

APPENDIX B

This appendix gives the details for interfacing the spectrofluorometer with the computer. The spectrofluorometer outputs the emission wavelength (λ_m) and the excitation wavelength (λ_x) through digital displays and through 0 V to 5 V analog signals. The digital display essentially provides the angular setting of the precision grating of the monochromator via a leadscrew. The leadscrew is attached to a potentiometer to provide a voltage output for the wavelength. The emission wavelength and the excitation wavelength shown in the digital display of the spectrofluorometer were each calibrated against their output voltages from the spectrofluorometer, v_m and v_x, respectively. Both the emission and the excitation wavelengths were each randomized with respect to run sequence. The emission and excitation calibration wavelengths and voltages are shown in Tables B.1 and B.2, respectively. The expanded uncertainty of the emission and excitation calibrations was less than 1 nm. All of the reported wavelengths were obtained from the voltage measurements via the calibration. Visual comparisons between the display wavelength and the wavelength obtained from the calibration were made periodically to ensure valid wavelength measurements.

Table B.1 Calibration data for excitation wavelength
File: xwavcal.dat

Run Number	Excitation wavelength (nm)	Volts
1	454	3.91054333333
2	343	2.99613666667
3	203	1.8363
4	654	5.57070666667
5	708	6.02836333333
6	721	6.13673666667
7	321	2.8111
8	299	2.63147
9	84	.843392666667
10	565	4.8441
11	863	7.31616666667
12	473	4.0692
13	747	6.35028
14	781	6.63456333333
15	59	.642042666667
16	20	.317264333333
17	238	2.12362333333
18	120	1.13697333333
19	815	6.91049
20	763	6.48913666667
21	779	6.6174
22	207	1.86744
23	97	.942503666667
24	60	.645223666667
25	107	1.02862
26	96	.935857666667
27	797	6.76124666667
28	640	5.45811666667
29	336	2.9379
30	848	7.18833666667
31	678	5.77650333333
32	149	1.38153
33	123	1.16183333333
34	539	4.62579333333
35	229	2.0503
36	516	4.43601333333
37	413	3.57772
38	168	1.5422
39	62	.660526
40	621	5.30198666667
41	617	5.26703333333
42	5	.184553333333
43	321	2.8102
44	760	6.46151
45	347	3.03109666667
46	599	5.12421
47	250	2.22018
48	211	1.90131666667
49	489	4.2043
50	460	3.96620333333
51	75	.766043
52	363	3.16579333333
53	46	.530862666667
54	190	1.72792333333
55	568	4.86575666667
56	59	.635964333333
57	322	2.82238333333
58	601	5.13819
59	285	2.5106
60	57	.620183333333
61	433	3.74113
62	176	1.61036666667
63	277	2.44536333333
64	597	5.11011
65	157	1.44956
66	751	6.38695666667
67	426	3.68207333333
68	84	.840409666667
69	334	2.91918333333
70	81	.812707
71	409	3.54545
72	213	1.9198
73	826	7.00214333333
74	637	5.43525666667
75	875	7.41642
76	648	5.51985666667
77	475	4.08714333333
78	834	7.07018666667
79	404	3.50418
80	145	1.34749
81	841	7.12723
82	720	6.12764333333
83	689	5.87079666667
84	573	4.90741
85	377	3.27737666667
86	763	6.48428333333
87	381	3.31445666667
88	476	4.09283333333
89	394	3.4255
90		

Table B.2 Calibration data for emission wavelength
File: mcordat2.dat

Run number	Emission wavelength (nm)	Volts
1	454	4.00459666667
2	343	3.06532
3	203	1.8902
4	654	5.68147333333
5	708	6.14710333333
6	721	6.25779
7	321	2.87878333333
8	299	2.69523
9	84	.898718
10	565	4.93474
11	863	7.44464666667
12	473	4.15744333333
13	747	6.4688
14	781	6.75045
15	59	.68113
16	20	.350998666667
17	238	2.18375666667
18	120	1.18951666667
19	815	7.0358
20	763	6.60640666667
21	779	6.74123333333
22	207	1.92390666667
23	97	.996606666667
24	60	.687480333333
25	107	1.07615966667
26	96	.993405
27	797	6.89357666667
28	640	5.55946
29	336	3.00727666667
30	848	7.32060333333
31	678	5.88147333333
32	149	1.43473
33	123	1.2112
34	539	4.71996666667
35	229	2.10741666667
36	516	4.52153333333
37	413	3.65250666667
38	168	1.59340333333
39	62	.708812666667
40	621	5.41223666667
41	617	5.37869333333
42	5	.225478666667
43	333	2.9835
44	760	6.57133666667
45	347	3.10932
46	599	5.23037333333
47	250	2.28521666667
48	211	1.9573
49	489	4.29196333333
50	460	4.05659666667
51	75	.813371
52	363	3.24532666667
53	46	.562347
54	188	1.77070666667
55	190	1.78293
56	568	4.96026333333
57	59	.684228666667
58	322	2.89331333333
59	601	5.24390333333
60	285	2.5758
61	57	.657163666667
62	433	3.82661333333
63	176	1.6578
64	277	2.51499666667
65	597	5.20722
66	157	1.50169
67	751	6.50546
68	426	3.76065
69	84	.887085666667
70	334	3.00055666667
71	81	.862142
72	409	3.61850666667
73	213	1.9732
74	826	7.13326333333
75	637	5.53811333333
76	875	7.54624333333
77	648	5.62997
78	475	4.17341
79	834	7.20676
80	404	3.57926666667
81	145	1.40417
82	841	7.26493
83	720	6.23879333333
84	689	5.9788
85	573	5.00254
86	377	3.35038333333
87	763	6.60635333333
88	381	3.38627666667
89	476	4.18624
90	394	3.49631

APPENDIX C

This appendix discusses how the emission and excitation wavelength measurements were verified with a mercury standard and a "crossover peak" from the excitation. The emission wavelength measurement obtained from the spectrofluorometer without the glass filter was checked against a mercury vapor light. Figure C.1 and Table C.1 show a comparison of the published values of the peak wavelengths for mercury (Reader et al., 1980) to those obtained from the spectrofluorometer. The absolute difference between the measured and published wavelengths was approximately within ± 2.5 nm, which was the width of the slits in the spectrofluorometer.

The excitation wavelength measurement obtained from the spectrofluorometer was checked with a "crossover peak" from the excitation. In other words, the excitation monochromator was set to a specific wavelength with no specimen in the sample chamber. Under these conditions, the emission intensity should peak at the excitation wavelength. The wavelength of the emission peaked at the excitation wavelength to within the resolution of the digital display (± 1 nm) for the wavelengths that were tested.

Table C.1 Calibration check of spectrofluorometer against Mercury lamp

Published[1] wavelength (nm)	Measured wavelength (nm)	Fluorescence intensity (% of max)	Absolute difference (nm)	Relative Difference (%)
312.567	310	0.004	2.567	0.80
365.015	363	0.014	2.015	0.55
404.656	402	0.045	2.656	0.66
435.833	435	0.128	0.833	0.19
546.074	545	0.079	1.074	0.20
576.960	578	0.045	-1.04	-0.18

[1]Reader et al. (1980)

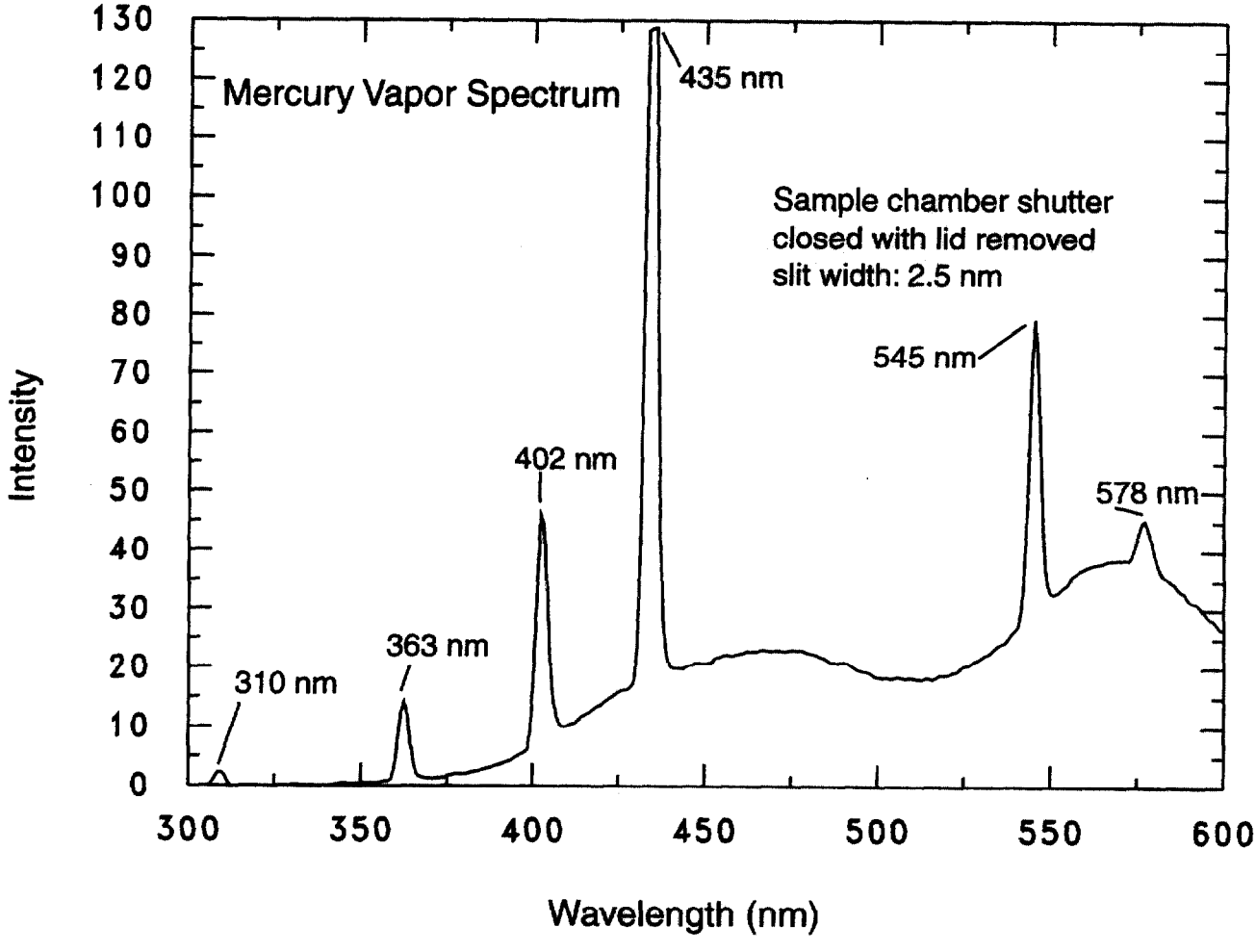

Fig. C.1 Verification of spectrofluorometer wavelength with Mercury standard

APPENDIX D

This appendix presents the measurements and the correlation of the York-C™ lubricant liquid density (ρ_b). The density of the liquid lubricant was measured as a function of temperature with a glass pycnometer. The pycnometer was factory instrumented with a glass mercury thermometer with a range of 14°C to 38°C in 0.2° graduations, accurate to within ±0.2 K. The pycnometer was filled with distilled water and its volume was calculated from the known density of water. The volume was found over five trails to be 9.84 ml with a standard uncertainty of 0.01 ml.

The pycnometer containing York-C™ was cooled in an ice bath and then removed from the bath and allowed to warm on the balance to room temperature over approximately one hour. The standard uncertainty of the balance was approximately 1 mg. The outside of the pycnometer was wiped clean before each measurement to remove the lubricant that was expelled through the pipette due to volume expansion with temperature increase.

The Biot number for the warming pycnometer was estimated to be approximately 0.5, which is greater than the recommended limit of 0.1 (Incropera and Dewitt, 1985) for a uniform temperature in fluid. It is difficult to estimate the error introduced in the measurements due to temperature gradients that existed in the lubricant. However, the data regression shows that the residuals are independent of temperature, which suggests that the error due to temperature gradients in the liquid had negligible on the density measurements.

Table D.1 shows the recorded measurements for two days. Equation D.1 gives the fit of the liquid lubricant density (ρ_L) in kg/m^3 versus temperature (T) in Kelvin:

$$\rho_L = 1076.7 - 0.572T \qquad \text{D.1}$$

The expanded uncertainty of the fit was approximately ± 1 kg/m^3 for 95 % confidence.

Table D.1 York-C™ liquid density measurements

T (°C)	g	ρ_L (kg/m^3)
0	9.048	919.8
15.8	8.955	910.3
17.2	8.934	908.2
20	8.926	907.4
21.2	8.922	907.0
22.4	8.916	906.4
24	8.906	905.3
25	8.901	904.8
0	9.057	920.7
15	8.967	911.6
18	8.941	908.9
19.2	8.93	907.8
21.6	8.919	906.7
22.2	8.917	906.5
22.8	8.911	905.9
23.6	8.907	905.4
24.8	8.901	904.8

APPENDIX E

This appendix gives a sample calculation of the ratio of the absorption of the incident excitation in the bulk to that in the excess layer (I_{oe}/I_{ob}). The absorption of a R123/York-C™ (95/5) mass fraction mixture was measured in an ultraviolet/visible absorption spectrometer and is shown is Fig. 9.

The Beer-Lambert Law (Amadeo et al., 1971) relates the absorbance (A) to the ratio of the incident light intensity (I_o) to the transmitted light intensity (I_t), i.e.,

$$A = \varepsilon c l = \log_{10} \frac{I_o}{I_t} \qquad \text{E.1}$$

The absorbance of a R123/York-C™ (99.5/0.5) mass fraction mixture can be calculated from that of the (95/5) mixture:

$$\frac{A_5}{A_{0.5}} = \frac{c_5}{c_{0.5}} = \frac{x_{m_5}\rho_{m_5}}{x_{m_{0.5}}\rho_{m_{0.5}}} = \frac{0.05\left(1436\text{kg/m}^3\right)}{0.005\left(1512\text{kg/m}^3\right)} = 9.5 \qquad \text{E.2}$$

The absorption for a 0.5 % mass mixture at 380 nm can be calculated the absorption for the 5 % mass mixture (1.42) and eq E.2 as:

$$A_{0.5} = A_5 \frac{A_{0.5}}{A_5} = \frac{1.42}{9.5} = 0.149 \qquad \text{E.3}$$

The product of ε and c for the 0.5 % mass mixture at 380 nm can be calculated from eq E.1:

$$\varepsilon c = \frac{A_{0.5}}{l_c} = \frac{0.149}{5\text{mm}} = 0.03\text{mm}^{-1} \qquad \text{E.4}$$

where the absorption length (l_c) is the internal thickness of the cuvette that was used absorption spectrometer.

The absorption ratio I_o/I_t can be calculated from the εc product and eq E.1 with the absorption length l equal to the distance between the bottom of the glass tube and the copper surface, i.e.,

$$\frac{I_o}{I_t} = 10^{\varepsilon c l} = 10^{0.03\text{mm}^{-1}1.46\text{mm}} = 1.10 \qquad \text{E.5}$$

For the optical bundle, the incident intensity is equal (I_o) is equal to the incident intensity for the bulk fluid (I_{ob}). Similarly, the transmitted intensity of eq E.5 is equal to the incident intensity for the excess layer (I_{oe}). Accordingly, the ratio of the absorption of the incident excitation in the bulk to that in the excess layer (I_{oe}/I_{ob}) for the 0.5 % mass mixture at 380 nm excitation is:

$$\frac{I_{oe}}{I_{ob}} = \frac{1}{1.10} = 0.9 \qquad \text{E.6}$$

The same calculation for I_{oe}/I_{ob} was done for the 1 % and 1.78 % mass mixtures for a 380 nm excitation and where found to be 0.82 and 0.71, respectively.